



Published  
for the  
International  
Glaciological  
Society

THIS MANUSCRIPT HAS BEEN SUBMITTED TO THE JOURNAL OF  
GLACIOLOGY AND HAS NOT BEEN PEER-REVIEWED.

**Observing glacier dynamics with low-cost, multi-GNSS  
positioning in Victoria Land, Antarctica**

Journal:	<i>Journal of Glaciology</i>
Manuscript ID:	Draft
Manuscript Type:	Article
Date Submitted by the Author:	n/a
Complete List of Authors:	Still, Holly; University of Otago, School of Surveying Odolinski, Robert; University of Otago, School of Surveying Bowman, M; University of Otago, Geology Hulbe, Christina; University of Otago, School of Surveying Prior, David; University of Otago, Geology
Keywords:	Glaciological instruments and methods, Antarctic glaciology, Glacier monitoring, Ice dynamics
Abstract:	This study examines the performance of low-cost, low-power GNSS positioning systems for glacier monitoring in high-latitude environments. We compare the positioning performance of co-located low-cost u-blox ZED-F9P GNSS units (~\$300 USD) and survey-grade Trimble R10 units (>\$15,000 USD, used) under stationary (on land) and dynamic (on glacier) conditions near Terra Nova Bay, Antarctica. Low-cost and survey-grade systems yield almost identical error magnitudes under short (3 m), medium (33 km) and long (390 km) baseline kinematic-positioning scenarios. We further examined the efficacy of low-cost GNSS for glaciological applications by installing four u-blox and two Trimble receivers on Priestley Glacier to observe tide-modulated ice flexure. All receivers successfully detected subtle tidal oscillations with amplitudes <3 cm, consistent with the predicted phasing from a tide model. These experiments offer a strong rationale for the widespread use of low-cost receivers to expand and densify GNSS monitoring networks, both in Antarctica and in glaciated regions worldwide.



SCHOLARONE™  
Manuscripts

# Observing glacier dynamics with low-cost, multi-GNSS positioning in Victoria Land, Antarctica

Holly STILL,<sup>1</sup> Robert ODOLINSKI,<sup>1</sup> M. Hamish BOWMAN,<sup>2</sup> Christina HULBE<sup>1</sup> David J. PRIOR<sup>2</sup>

<sup>1</sup>*School of Surveying, University of Otago, Dunedin, NZ*

<sup>2</sup>*Department of Geology, University of Otago, Dunedin, NZ*

*Correspondence:* Holly Still <holly.still@otago.ac.nz>

## ABSTRACT.

This study examines the performance of low-cost, low-power GNSS positioning systems for glacier monitoring in high-latitude environments. We compare the positioning performance of co-located low-cost u-blox ZED-F9P GNSS units (~\$300 USD) and survey-grade Trimble R10 units (>\$15,000 USD, used) under stationary (on land) and dynamic (on glacier) conditions near Terra Nova Bay, Antarctica. Low-cost and survey-grade systems yield almost identical error magnitudes under short (3 m), medium (33 km) and long (390 km) baseline kinematic-positioning scenarios. We further examined the efficacy of low-cost GNSS for glaciological applications by installing four u-blox and two Trimble receivers on Priestley Glacier to observe tide-modulated ice flexure. All receivers successfully detected subtle tidal oscillations with amplitudes <3 cm, consistent with the predicted phasing from a tide model. These experiments offer a strong rationale for the widespread use of low-cost receivers to expand and densify GNSS monitoring networks, both in Antarctica and in glaciated regions worldwide.

## 1 INTRODUCTION

Ice displacement and velocity are fundamental measurements used in glaciology to investigate ice mechanics and to constrain ice flow models. Observations of ice displacement are often obtained *in situ* using Global Navigation

26 Satellite Systems (GNSS), which can provide high-precision horizontal and vertical positioning and precise timing  
27 information. Applications in Antarctica include the measurement of ice velocity and strain rate (Hulbe and Whillans,  
28 1994; Minowa and others, 2019; Klein and others, 2020), observation of vertical land motion (Thomas and others,  
29 2011; Zanatta and others, 2017; King and others, 2022), validation of satellite and radar ice altimetry data (Brenner  
30 and others, 2007; Schröder and others, 2017; Brunt and others, 2019), and mapping ice surface topography and  
31 surface elevation change (Hulbe and Whillans, 1997; Spikes and others, 2003; Richter and others, 2014). GNSS  
32 positioning is used to provide location and contextual information for transmitters and receivers used for geophysical  
33 remote sensing techniques, including radar sounding (Horgan and others, 2017; Pratap and others, 2022), passive  
34 and active-source seismic sounding (Minowa and others, 2019; Huang and others, 2022), and gravity measurements  
35 (Zanatta and others, 2017). It is used to locate sample collection sites, including ice cores and ice-anchored moorings  
36 (Arzeno and others, 2014; Thomas and others, 2021). Many of these applications require (or could benefit from) a  
37 network of multiple GNSS devices deployed, yet this is costly and logistically challenging in polar environments.

38 Glaciological applications typically use geodetic or survey-grade GNSS receivers and antennas (e.g., Siegfried and  
39 others, 2016; Cooley and others, 2019; Brunt and others, 2019; Still and others, 2022). These systems are robust,  
40 reliable, and can provide dual or triple frequency, multi-GNSS data at a high rate ( $\geq 1$  Hz), leading to centimetre-level  
41 horizontal and vertical precision under ideal conditions. However, these systems are also expensive. State-of-the-art  
42 survey-grade GNSS receiver and antenna systems retail for  $\sim \$30,000$  USD, and refurbished last-generation systems  
43 were available for  $\sim \$10,000$  USD at the time of writing (AllTerra, 2023). High equipment costs can be prohibitive to  
44 scientific discovery, limiting the concurrent deployment of multiple GNSS receivers over large areas of interest and  
45 restricting access to users with well-financed research programs (e.g., Chagas, 2018; Oellermann and others, 2022).  
46 Additional limitations of survey-grade receivers for deployment in remote environments include high rates of power  
47 consumption, the size and weight of receivers and antennas, and the weight of battery banks needed for multi-day  
48 installations (Willis, 2008; Jones and others, 2016).

49 Low-cost, mass-market GNSS chip devices – a relatively new and rapidly developing technology – are a promising  
50 alternative to the GNSS units typically used in glacier studies. These low-cost systems retail for less than 10% of  
51 the cost of survey-grade alternatives (AllTerra, 2023; U-blox, 2023). Coupled with a low-cost patch antenna and  
52 data logger, low-cost GNSS units are light and compact, with relatively low power consumption (e.g., Jones and  
53 others, 2016). Low-cost receivers and antennas can achieve centimetre-level precision by tracking multiple GNSS  
54 satellite constellations (e.g., GPS, GLONASS, Galileo, Beidou, QZSS) at two or more carrier frequencies (Odolinski  
55 and Teunissen, 2016, 2020). The low-cost u-blox ZED-F9P GNSS receiver, for example, has a specified real time

56 kinematic (RTK) positioning accuracy of 1 cm + 1 ppm over a 1 km baseline (U-blox, 2022c) in optimal conditions.  
57 In practice, the positioning performance depends on baseline length (the distance between a reference station and  
58 moving GNSS receiver), satellite–receiver geometry, antenna and receiver hardware design, atmospheric conditions,  
59 and multipath interference errors (Odijk and Wanninger, 2017, pg. 770–773), all of which are relevant to polar  
60 applications. The performance of readily-available u-blox ZED-F9P receivers is investigated here as a low-cost  
61 solution for glacier monitoring.

62 The precision and reliability of low-cost GNSS receivers has been evaluated for short baseline, static and dynamic  
63 positioning at mid to low latitudes (e.g., Odolinski and Teunissen, 2016; Nie and others, 2020; Xue and others,  
64 2022). Similar performance comparisons between low-cost and survey-grade systems have not been conducted in  
65 high-latitude, glaciated environments. Of relevance to polar environments where permanent GNSS reference stations  
66 are sparse, Odolinski and Teunissen (2020) show that the positioning performance of u-blox ZED-F9P receivers is  
67 competitive with a survey-grade system in a long-baseline (112.9 km), kinematic positioning configuration. Per-  
68 formance evaluations of the u-blox ZED-F9P GNSS module in geophysical monitoring contexts have also yielded  
69 millimetre-level precision for continuous tectonic motion (Tunini and others, 2022) and landslide detection (Šegina  
70 and others, 2020; Notti and others, 2020). In controlled kinematic experiments, u-blox ZED-F9P receivers paired with  
71 low-cost antennas could detect mechanically-induced horizontal displacements as small as 10 mm (RTK positioning,  
72 short <100 m baseline, clear sky conditions) (Hamza and others, 2020; Hohensinn and others, 2022). All of these  
73 results suggest that the measurement precision needed for glacier mechanics studies is possible with this equipment,  
74 and for this reason, u-blox GNSS hardware is evaluated in the present study.

75 Polar environments present challenges, limitations, and sources of error that can affect the positioning performance  
76 of both low-cost and survey-grade GNSS equipment. At high latitudes, maximum satellite elevations are lower in the  
77 sky, with no satellites passing directly overhead (Zhang and others, 2020; Di and others, 2022). This weaker satellite–  
78 receiver geometry can lead to an unfavourable vertical dilution of precision and larger vertical positioning errors  
79 (Hugentobler and Montenbruck, 2017; Alkan and others, 2022). A second source of error, multipath interference,  
80 occurs when transmitted signals are deflected off objects before reaching the receiver. Highly reflective snow and  
81 ice surfaces may amplify multipath errors, particularly when satellites are at low elevations above the horizon (e.g.,  
82 Benton and Mitchell, 2011; Nievinski and Larson, 2014). A third source of error originates from the degradation of  
83 GNSS signals due to geomagnetic and ionospheric storms. These space weather disturbances have a greater intensity  
84 at high latitudes, near the magnetic poles (Linty and others, 2018; Nie and others, 2022; Paziewski and others, 2022).  
85 Altogether, these error sources and the presence of low elevation satellites can affect positioning performance by

decreasing the GNSS receiver signal-to-noise ratio and increasing the frequency of cycle slips, a temporary loss-of-lock on a satellite (Dabove and others, 2020; Di and others, 2022).

Performance evaluations of GNSS receivers are often undertaken in controlled, open-sky environments with favourable conditions to achieve optimal precision and accuracy. These conditions can include: a satellite–receiver geometry that minimises positioning errors, calm ionospheric conditions, short baselines (<50 km), and mitigation of low-elevation multipath errors. This study evaluates low-cost GNSS positioning performance in a high-latitude, glaciated environment in Antarctica under challenging conditions, including medium to long baselines, varying ionospheric conditions, a glacier-valley site with some loss of sky view, a highly reflective snow or ice surface, sub-zero temperatures and differing receiver and antenna models for the base station and rover. An important objective is to evaluate whether the performance of low-cost GNSS is suitable for glaciological applications that require centimetre-level precision (e.g., the detection of velocity variability over timescales of hours to days).

## 1.1 Objectives

This study analyses the performance of low-cost, low-power GNSS positioning for glacier and ice sheet monitoring applications in high-latitude environments. We compare the performance of u-blox ZED-F9P GNSS receivers (<\$300 USD) and survey-grade Trimble R10 receivers (>\$10,000 USD purchased second-hand; >\$40,000 USD new) under stationary (on land) and dynamic (on glacier) conditions near Terra Nova Bay, Antarctica. In each experiment, u-blox and Trimble receivers were installed alongside each other to record positions simultaneously under the same satellite geometry and environmental conditions. The u-blox receivers were paired with both low-cost patch antennas and standard surveying antennas while the Trimble R10 receivers were used with their integrated antenna.

Three experiments were performed. The first experiment compares and evaluates performance under stationary conditions on stable ground near Mario Zucchelli Station in Terra Nova Bay, Antarctica (Fig. 1). This short baseline (3 m) experiment establishes the optimal expected performance of the receivers at a high-latitude site. The second experiment compares and evaluates the performance under dynamic conditions on Priestley Glacier. One Trimble and two u-blox receivers were installed alongside each other on an advecting ice surface. We evaluate the kinematic positioning solutions for both medium (34 km) and long baselines (390 km). The third experiment evaluates performance in a realistic glacier monitoring context: measuring the tidal flexure of Priestley Glacier's shear margin. Six GNSS units (4 u-blox, 2 Trimble) were installed in across- and along-flow transects near the margin of Priestley Glacier (Fig. 1).

Single-baseline kinematic positioning solutions are used in the present work. That is, we determine the trajectory

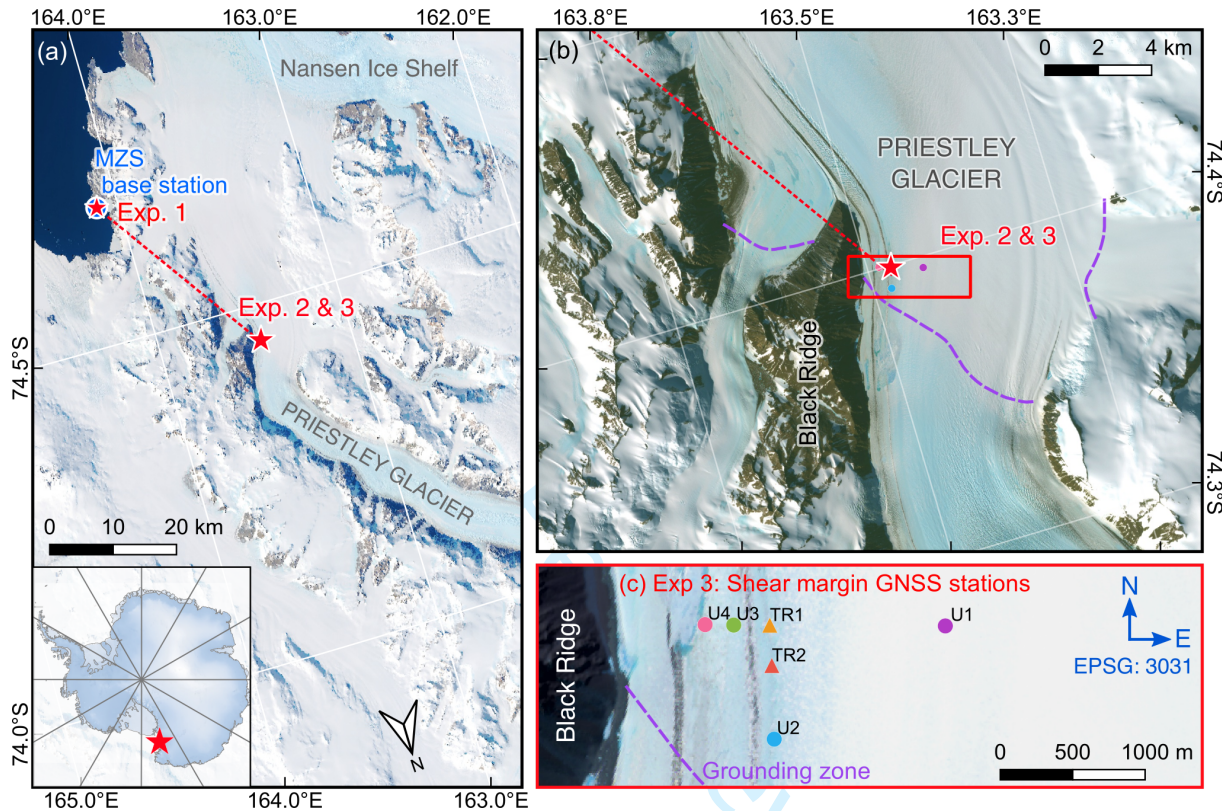


**Fig. 1.** Site map of GNSS experiments conducted near Terra Nova Bay in the Ross Sea region, Antarctica. Map (a): the location of the stationary GNSS experiment (Experiment 1) at Mario Zucchelli Station (MZS), and the dynamic GNSS experiments on Priestley Glacier (Experiments 2 and 3). Map (b): the field site near Priestley Glacier's left lateral margin, approximately 1 km downstream from the grounding zone. Map (c): the locations of u-blox (U) and Trimble (TR) GNSS stations installed across the shear margin (Experiment 3). The estimated location of the grounding zone is from Rignot and others (2016) and the basemaps contain modified Sentinel-2, 10 m resolution imagery acquired on December 18, 2022, courtesy of the European Space Agency.

of a moving GNSS antenna (the ‘rover’) relative to a single stationary base station receiver. This is a relative positioning technique and the ‘baseline’ is the distance between the rover and a base station. The technique requires simultaneous observations from the two receivers, one of which is installed on stationary terrain. Relative positioning eliminates satellite and receiver clock errors, and reduces errors associated with satellite orbits, ionospheric, and tropospheric delays. Centimetre-level or better precision is achievable providing that integer ambiguity resolution is used.

An alternative positioning method, precise point positioning (PPP), requires the deployment of only a single GNSS receiver (Zumberge and others, 1997; Kouba and Héroux, 2001). PPP is commonly used in remote polar environments where logistical difficulties or lack of access to stationary terrain are barriers to the installation of temporary base stations. Permanent GNSS reference stations in Antarctica are sparse, distributed near coastlines, and may be located hundreds of kilometres away from field sites. Both single-baseline kinematic positioning and PPP have produced centimetre-level precision in Antarctica, using survey-grade equipment (Richter and others, 2014; Schröder and others, 2017; Still and others, 2022; Li and others, 2019; Alkan and others, 2022). The quality of a PPP solution, however, depends on precise orbit and clock products, and the convergence time (hours rather than minutes) is significantly longer compared to relative positioning methods. If the goal is to achieve very precise 3D positions and velocities, a single-baseline kinematic positioning solution is expected to be the best-performing technique in a short to medium baseline configuration (i.e., less than 100 km between base station and rover).

## 2 METHODS

### 2.1 Low-cost GNSS instrumentation

Each low-cost GNSS installation includes a receiver, antenna, data logger and power source (12 V battery and solar panel) (Table 1). The u-blox ZED-F9P GNSS receiver module is capable of tracking GPS (L1/L2), GLONASS (L1/L2), Galileo (E1/E5b), Beidou (B1/B2), and QZSS (L1/L2) systems and frequencies (U-blox, 2022c). The ZED-F9P module operates over a wide temperature range ( $-40^{\circ}\text{C}$  to  $85^{\circ}\text{C}$ ) and the rate of power consumption is relatively low (0.57 W for the u-blox ZED-F9P module + patch antenna + Arduino Cortex M0 logger, versus 1.25 W for a Trimble R10 system, and 3.67 W for a Trimble NetR9 system). The receiver is configured to log all available satellites and frequencies at 1 Hz using the software U-center v22.07 (U-blox, 2022b). RXM-RAWX messages (raw carrier phase, pseudorange, Doppler and signal quality information) and RXM-SFRBX messages (broadcast navigation data) are enabled and the raw binary u-blox files are stored with an Arduino data logger to micro SD card.

144 Two low-cost multiband antenna models are trialled with the u-blox receivers: the u-blox ANN-MB patch antenna  
145 (U-blox, 2022a) and an Eltehs multiband (ELT0123) standard surveying antenna (GNSS OEM, 2023) (Table 1).  
146 Patch antennas are designed to attach to flat surfaces and have magnetic bases for this purpose. We attach our patch  
147 antennas to 0.12 m diameter circular steel plates fabricated for these experiments. The plates act as a ground plane  
148 that reduces multipath interference for the otherwise exposed antennas (U-blox, 2019; Punzet and Eibert, 2023). In  
149 Experiments 1 and 2, the ground plates are bolted onto tripods. In Experiment 3, the plates are attached to uPVC  
150 glacier stakes with 5/8" inch screws. The stakes are frozen into holes drilled vertically into the ice. All antennas  
151 used in the experiments are aligned to true north to compensate for the offset error associated with any differences  
152 between the antenna phase centre and physical centre (Wolf and Ghilani, 2006, p.g., 388). The low-cost GNSS units  
153 are powered by two 10 W, 12 V solar panels and a 12 V, 18 A h SLA battery.

## 154 2.2 Low-cost and survey-grade GNSS data processing

155 The first processing step involves a conversion from the proprietary u-blox and Trimble raw data file formats to  
156 standard RINEX 3.03 (Receiver Independent Exchange) files. U-blox data streams are converted using open-source  
157 RTKLIB tools (Takasu and Yasuda, 2009). Trimble observation files were converted using the Trimble ‘Convert to  
158 RINEX’ utility, version 3.1.4.0. GNSS stationary and dynamic observations are post-processed using the RTKPOST  
159 module within RTKLIB v2.4.3 b34 (Takasu and Yasuda, 2009; Takasu, 2013).

160 Multi-GNSS (GPS, GLONASS, Galileo, Beidou and QZSS) pseudorange and carrier phase measurements are  
161 post-processed in kinematic mode using RTKLIB. A satellite elevation cut-off angle of 15° is applied to mitigate  
162 low-angle multipath or atmospheric errors. Solutions are computed at a 1 second measurement interval for short  
163 baselines (Experiment 1) to demonstrate that the low-cost system is capable of high-rate (1 Hz) data logging in  
164 this environment. For medium and long baselines (Experiments 2 and 3), solutions are computed at a 10 second  
165 measurement interval to avoid reported time correlations of several seconds in the code observations for u-blox  
166 receivers (Odolinski and Teunissen, 2020), which if neglected, can significantly affect positioning results. This is  
167 particularly true for medium and long baselines when relative atmospheric delays enter the model (Odolinski, 2012).

168 Base station and rover pairs are listed in Table 2 and kinematic processing techniques and parameters are sum-  
169 marised in Table 3. RTKLIB configuration settings are modified to improve the solutions for short, medium, or long  
170 baselines (e.g., Odolinski and others, 2015b). Identical processing settings are applied to each base-rover pair within  
171 each experiment and are not modified to suit a low-cost or survey-grade receiver or antenna, ensuring a fair perfor-  
172 mance comparison between the different solutions. Daily multi-GNSS broadcast ephemeris files (the BRDM00DLR\*

**Table 1.** Specifications of the GNSS receiver and antenna hardware evaluated in each experiment. All frequency bands supported by the GNSS receivers are listed. Frequencies in bold font are used in the three experiments for a fairer comparison between u-blox and Trimble systems. Power consumption estimates are from measurements rather than manufacturer specifications. Low-cost equipment prices are from the GNSS OEM Store (<https://gnss.store/content/4-about-us>) and survey-grade equipment pricing is from AllTerra (2023).

Receiver/antenna	u-blox ZED-F9P + multiband patch antenna	u-blox ZED-F9P + multiband surveying antenna	Trimble R10 (integrated antenna)
Systems and frequencies (receiver)	GPS: <b>L1, L2</b> GLO: <b>L1, L2</b> GAL: <b>E1, E5b</b> BDS: <b>B1, B2</b> QZSS: <b>L1, L2</b>	GPS: <b>L1, L2</b> GLO: <b>L1, L2</b> GAL: <b>E1, E5b</b> BDS: <b>B1, B2</b> QZSS: <b>L1, L2</b>	GPS: <b>L1, L2, L5</b> GLO: <b>L1, L2, L3</b> GAL: <b>E1, E5b, E5a, E6</b> BDS: <b>B1, B2, B3</b> QZSS: <b>L1, L2, L5</b>
Dimensions (receiver, mm)	17.0 × 22.0 × 2.4	17.0 × 22.0 × 2.4	119 × 119 × 136
Dimensions (antenna, mm)	60.0 × 82.0 × 22.5	160.0 × 160.0 × 66.5	n/a
Weight (receiver)	< 100 g	< 100 g	1.12 kg
Weight (antenna)	173 g	400 g	n/a
Operating temp (receiver)	-40 °C to +85 °C	-40 °C to +85 °C	-40 °C to +65 °C
Operating temp (antenna)	-40 °C to +85 °C	-40 °C to +70 °C	n/a
Receiver price	\$187 USD	\$187 USD	> \$15,000 USD (used)
Antenna price	\$90 USD	\$199 USD	n/a
Power usage of GNSS system	0.57 W	0.65 W	1.25 W
Positioning accuracy (horiz)	0.01 m + 1 ppm CEP	0.01 m + 1 ppm CEP	0.008 m + 1 ppm RMS (RTK)
Antenna gain	28 dB	38 dB	50 dB
Experiment 1 (Fig. 2)	Rover + base station	n/a	Rover + base station
Experiment 2 (Fig. 6)	Rover (Ub2)	Rover (Ub1)	Rover (Tr1)
Experiment 3 (Fig. 1c)	Rover (Ub3, Ub4)	Rover (Ub1, Ub2)	Rover (Tr1, Tr2)

173 product) (Steigenberger and Montenbruck, 2020) from the CDDIS GNSS data archive (Noll, 2010) are used for short  
174 and medium baseline tests. Final multi-GNSS orbit and clock information (GFZ0OPSFIN\* products) from the GFZ  
175 Analysis Centre (Deng and others, 2016; Montenbruck and others, 2017) are used for the long baseline (390 km) test  
176 because satellite orbit errors enter the single-baseline positioning model as the baseline increases. Output positions  
177 are provided as WGS84 latitude, longitude and ellipsoidal height. Coordinates are transformed to the Antarctic  
178 Polar Stereographic coordinate system (EPSG:3031). Time series position data are presented with the mean position  
179 for each station removed.

180 Smoothing or filtering techniques are often applied to processed GNSS time series to remove unrealistic peaks  
181 and high frequency noise associated with multipath interference. In Experiment 3 (Fig. 1c), in which the objective  
182 is to observe ice flexure and tidal modulation of ice velocity, outliers are removed with a three-hour moving median  
183 filter to prevent unrealistic peaks in the horizontal and vertical position time series. This method defines outliers as  
184 points that fall beyond a threshold of three scaled median absolute deviations from the sliding median. No filtering,  
185 smoothing or outlier detection methods are applied to the solutions in Experiments 1 and 2 (Section 1.1). GNSS  
186 data are presented ‘as is’ for the comparisons between low-cost and survey-grade receivers.

### 187 3 EXPERIMENT 1: STATIONARY, SHORT-BASELINE POSITIONING

188 This experiment quantifies the uncertainty of GNSS positions obtained with low-cost u-blox systems and directly com-  
189 pares the performance of u-blox and Trimble receivers under the same environmental conditions. In a short-baseline  
190 positioning configuration, ionospheric and tropospheric errors, and satellite clock and orbit errors are negligible. This  
191 stationary, short-baseline experiment therefore demonstrates the optimal expected performance of the low-cost GNSS  
192 devices for polar applications.

193 The stationary comparisons of low-cost u-blox and survey-grade Trimble receivers were conducted at Mario Zuc-  
194 chelli Station, a coastal research station located on a granite promontory in Terra Nova Bay ( $74.6954^{\circ}$  S,  $164.0962^{\circ}$  E).  
195 Four GNSS units (2 low-cost u-blox F9P receivers and 2 survey-grade Trimble R10 receivers) were deployed in a base  
196 station and rover pair, on stationary ground, with a short baseline of 3.5 m (Fig. 2). Receivers and antennas were  
197 installed approximately 300 m up-slope from Mario Zucchelli Station to maximise sky view and avoid interference  
198 from buildings. Both u-blox receivers were equipped with ANN-MB patch antennas and ground plates. The Trimble  
199 R10 hardware consists of a receiver and ultra-compact Zephyr antenna within a single unit. Positions logged during  
200 the final 12 hours of the experiment, 0600 to 1800 hours (UTC) on 16 November, 2022, are analysed here. Positioning  
201 performance is evaluated in terms of the standard deviation for each component of position (east, north, up), and the

**Table 2.** Summary of GNSS positioning experiments conducted at Mario Zucchelli Station (Mzs) and on Priestley Glacier (PG). Experiment sites are mapped in Fig. 1. See Table 1 for instrument specifications.

Single-baseline kinematic positioning, u-blox versus Trimble comparisons						
	Baseline	Rover receiver + antenna	Base receiver + antenna	Duration	Rover site	Section
<b>Experiment 1</b> (Stationary)	3.5 m 3.5 m	u-blox F9P + patch Trimble R10	u-blox F9P + patch Trimble R10	13 hrs 13 hrs	Mzs Mzs	3.1
<b>Experiment 2</b> (Dynamic, medium baseline)	33 km 33 km 33 km	u-blox F9P + patch u-blox F9P + surveying Trimble R10	Trimble NetR9 + Zephyr Trimble NetR9 + Zephyr Trimble NetR9 + Zephyr	15 hrs 15 hrs 15 hrs	PG PG PG	4.1
<b>Experiment 2</b> (Dynamic, long baseline)	390 km 390 km 390 km	u-blox F9P + patch u-blox F9P + surveying Trimble R10	Trimble Alloy + Zephyr 3 Trimble Alloy + Zephyr 3 Trimble Alloy + Zephyr 3	15 hrs 15 hrs 15 hrs	PG PG PG	4.2
Application: kinematic positioning to monitor tidally-modulated ice flexure						
	Baseline	Rover receiver + antenna	Base receiver + antenna	Duration	Rover site	
<b>Experiment 3</b> (Dynamic)	33 km 33 km 33 km 33 km 33 km 33 km	Trimble R10 Trimble R10 u-blox F9P + patch u-blox F9P + patch u-blox F9P + surveying u-blox F9P + surveying	Trimble NetR9 + Zephyr Trimble NetR9 + Zephyr	8.5 days 7 days 4 days 4 days 3 days 3 days	PG PG PG PG PG PG	5

**Table 3.** RTKLIB configuration settings for post-processing of u-blox and Trimble position time series.

Setting	Short baseline	Medium baseline	Long baseline
Dynamic model for positions	None (kinematic)	None (kinematic)	None (kinematic)
Constellations	G, R, E, C, J	G, R, E, C, J	G, R, E
Frequencies	L1+L2	L1+L2	L1+L2
Filter type	Forward	Forward	Forward
Elevation mask	15°	15°	15°
Ionosphere correction	Broadcast	Estimate TEC	Estimate TEC
Troposphere correction	None	None	Estimate ZTD
Satellite Ephemeris/Clock	Broadcast	Broadcast	Precise
Dynamic model for ambiguities	Time constant	Time constant	Time constant

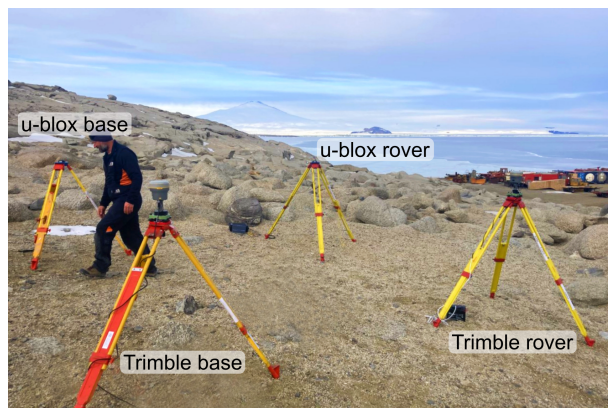


**Fig. 2.** Low-cost u-blox and survey-grade Trimble receivers and antennas in a short-baseline (3.5 m) configuration near Mario Zucchelli Station in Terra Nova Bay, Antarctica (Experiment 1).

202 2D (horizontal) and 3D (horizontal and vertical) root mean square (RMS) error, a collective measure of the difference  
203 between observed and expected positions. Statistics for each experiment are presented in Table 4.

### 204 3.1 Short-baseline positioning performance

205 The satellite visibility and geometry together affect the precision of the horizontal and vertical positions. Both u-blox  
206 and Trimble systems were configured to track five satellite systems visible in Antarctica (GPS, GLONASS, Galileo,  
207 Beidou, QZSS). With an elevation cutoff angle of 15°, the u-blox system tracked a mean of 31.8 satellites (minimum  
208 = 26, maximum = 39) and the Trimble system tracked a mean of 30.0 satellites (minimum = 24, maximum = 35).  
209 The difference is due to the improved continuous signal tracking of Beidou satellites by the u-blox receiver (Fig.  
210 3g-h). The positional dilution of precision (PDOP) is a measure of the strength of the receiver–satellite geometry.  
211 Lower PDOP values indicate a stronger geometry (i.e., satellites are well-distributed rather than clustered across  
212 the sky). The receivers experienced similar small excursions in PDOP (Fig. 3i-j), which is reflected as an increase  
213 in noise and poorer precision, particularly in the vertical component (for example, see the epochs at 0745 UTC for  
214 the Trimble solution, column 2). Overall, excellent PDOP values approaching 1 were observed for both u-blox and  
215 Trimble systems. A PDOP >10 indicates a poor receiver–satellite geometry (e.g., Teunissen and others, 2014).

216 The horizontal and vertical precisions of the two systems are nearly identical (Fig. 3). The horizontal root mean  
217 square ( $RMS_{2D}$ ) error is 2.4 mm for both the u-blox and Trimble GNSS stations (Table 4). The u-blox system also  
218 provided a marginal improvement in vertical precision in comparison to the Trimble system (u-blox:  $\sigma_u = 5.6$  mm vs.  
219 Trimble:  $\sigma_u = 5.9$  mm, Fig. 3). The corresponding 95% confidence ellipses are a 2D representation of the positional

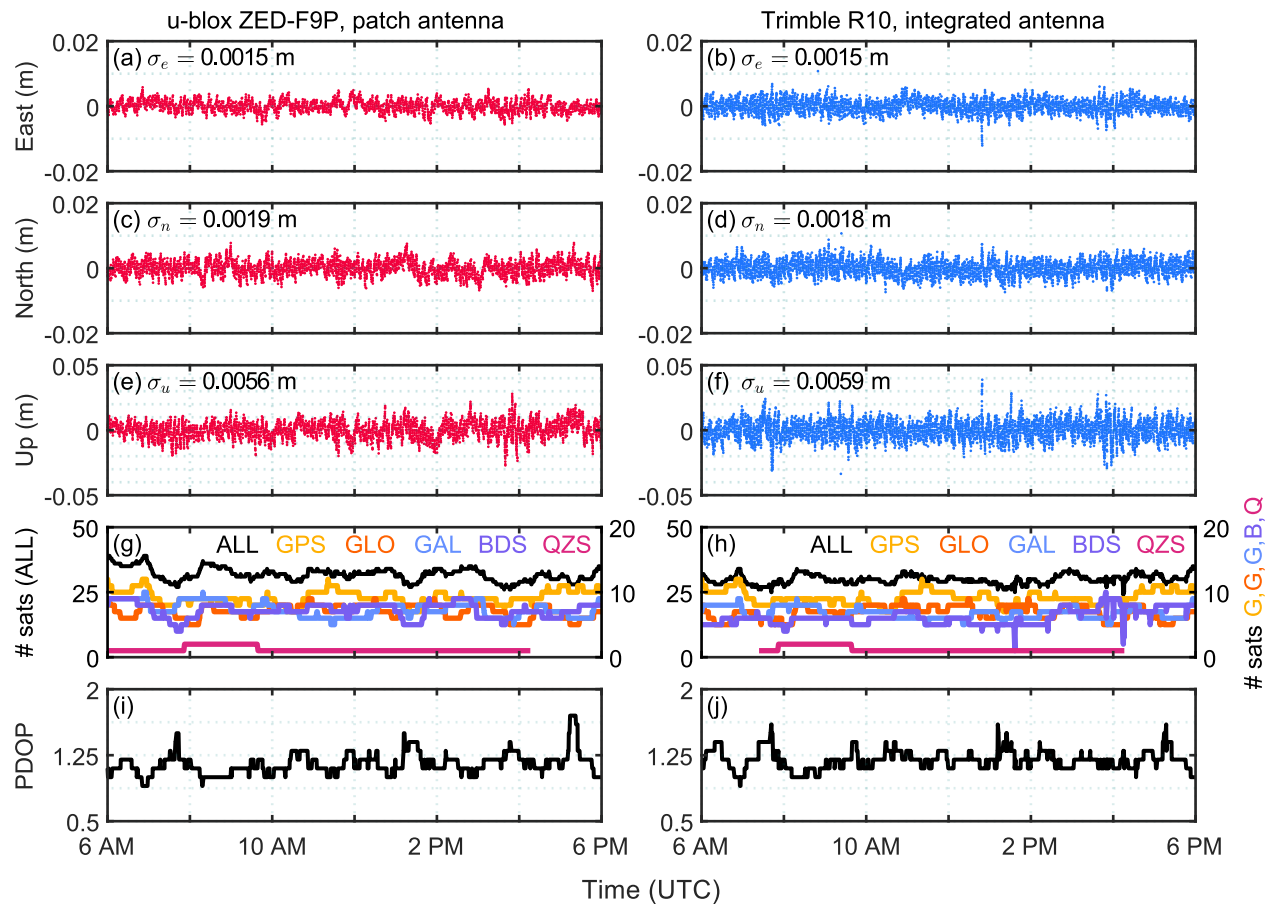


**Fig. 3.** Short baseline, static positions recorded with u-blox and Trimble GNSS stations over a 12 hour observation period on 16 November, 2022 (Experiment 1). East and north components of position correspond to the horizontal axes of the Antarctic Polar Stereographic coordinate system (EPSG:3031), with the mean position removed.  $n = 43,200$  epochs are included in each time series (1 Hz sample rate).  $\sigma$  is one standard deviation. The PDOP is the 3D position dilution of precision. Note the change in  $y$ -axis limits from  $\pm 2$  cm for the horizontal components to  $\pm 5$  cm for the vertical component.

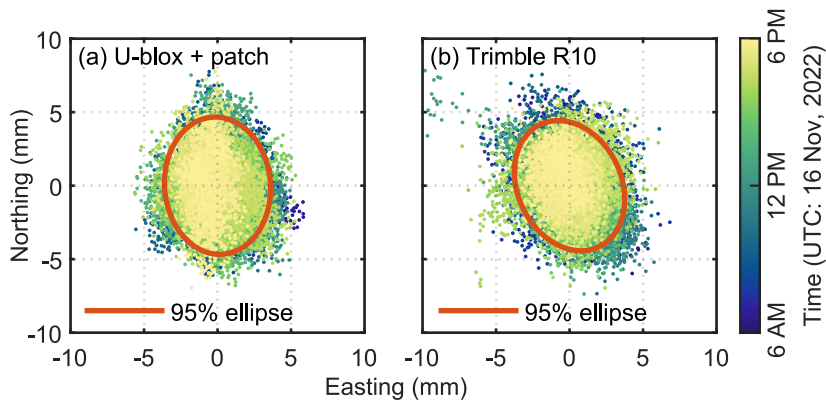


**Fig. 4.** Horizontal positions and 2D 95% confidence ellipses for the u-blox and Trimble position time series. Confidence ellipses are computed from  $n = 43,200$  positions obtained over 12 hours on 16 November, 2022. ‘North’ corresponds to grid north and the coordinate system is the same as in Fig. 3.

errors associated with the low-cost receiver (Fig. 4a). Positioning errors are of a similar magnitude for u-blox and Trimble systems (Ub: largest eigenvalue  $\lambda_1 = 3.6 \times 10^{-6}$  m, Tr:  $\lambda_1 = 3.1 \times 10^{-6}$  m). The approximate north–south orientations of the ellipse semi-major axes are consistent with fewer positioning satellites traversing the southern sky at a high latitude site. This geometrical configuration, where satellite trajectories are less frequent in the southern sky, is depicted by the skyplots presented in Fig. 5.

## 4 EXPERIMENT 2: DYNAMIC, MEDIUM AND LONG-BASELINE POSITIONING

This experiment evaluates the dynamic performance of the low-cost system in a glaciated setting. Two u-blox (Ub1 and Ub2) and one Trimble R10 (Tr1) GNSS station(s) were installed adjacent to each other on the floating left shear margin of Priestley Glacier (Fig. 6a). Station Ub1 was paired with a patch antenna (U-blox, 2022a) and Ub2 was paired with an alternative low-cost surveying antenna (GNSS OEM, 2023) (Fig. 6b and c) to assess whether low-cost antenna type affects positioning performance. The GNSS stations were aligned in a flow-oriented transect with a 5 m spacing. Antennas were installed 2 m above the ice surface with antenna centres positioned at the same elevation to ensure equivalent sky-view conditions. Positions were logged at a 1-second measurement interval for 15 hours during the neap tide on 21 November, 2022. Maximum windspeeds of 12 knots were recorded during the experiment.

The dynamic positioning performance of the u-blox and Trimble systems is evaluated for medium (33.9 km) and long (390 km) baseline configurations. A temporary base station (Trimble NetR9 receiver + Zephyr model antenna)

**Table 4.** The precision of u-blox and Trimble GNSS observations.  $\sigma_e$ ,  $\sigma_n$ , and  $\sigma_u$  denote the standard deviation of the easting, northing and vertical positions. For Experiment 2,  $\sigma_n$  is the standard deviation of the detrended northing positions (i.e., the mean downstream flow is removed). For Experiment 3 (dynamic observations), standard deviations  $\sigma_e$ ,  $\sigma_n$ , and  $\sigma_u$  are computed for 30-minute moving windows and presented as the mean for each time series. The 2D (horizontal) and 3D root mean square (RMS) errors are also computed for 30-minute moving windows and presented as the mean (Experiments 2 and 3). The mean position is taken as the reference value for each RMS error calculation.

		Receiver + antenna	$\sigma_e$ (mm)	$\sigma_n$ (mm)	$\sigma_u$ (mm)	RMS <sub>2D</sub> (mm)	RMS <sub>3D</sub> (mm)
<b>Experiment 1</b> (Stationary)	Ub	u-blox + patch	1.5	1.9	5.6	2.4	6.1
	Tr	Trimble R10	1.5	1.8	5.9	2.4	6.4
<b>Experiment 2</b> (Dynamic, medium) baseline)	Ub1	u-blox + surveying	7.0	9.6	24.4	8.4	20.2
	Ub2	u-blox + patch	8.4	9.2	26.9	9.7	23.2
	Tr1	Trimble R10	6.5	8.5	26.6	8.3	22.0
<b>Experiment 2</b> (Dynamic, long) baseline)	Ub1	u-blox + surveying	5.7	6.9	28.4	6.2	21.2
	Ub2	u-blox + patch	9.8	10.7	38.4	9.9	29.7
	Tr1	Trimble R10	5.3	7.5	37.4	6.5	22.4
<b>Experiment 3</b> (Dynamic, medium) baseline)	Ub1	u-blox + surveying	4.3	5.7	17.0	7.1	18.4
	Ub2	u-blox + surveying	4.8	6.4	15.9	8.1	17.8
	Ub3	u-blox + patch	5.1	6.7	19.4	8.7	21.1
	Ub4	u-blox + patch	5.1	6.3	18.6	8.3	20.3
	Tr1	Trimble R10	4.6	6.0	16.7	7.6	18.3
	Tr2	Trimble R10	4.0	5.5	15.0	6.9	16.5

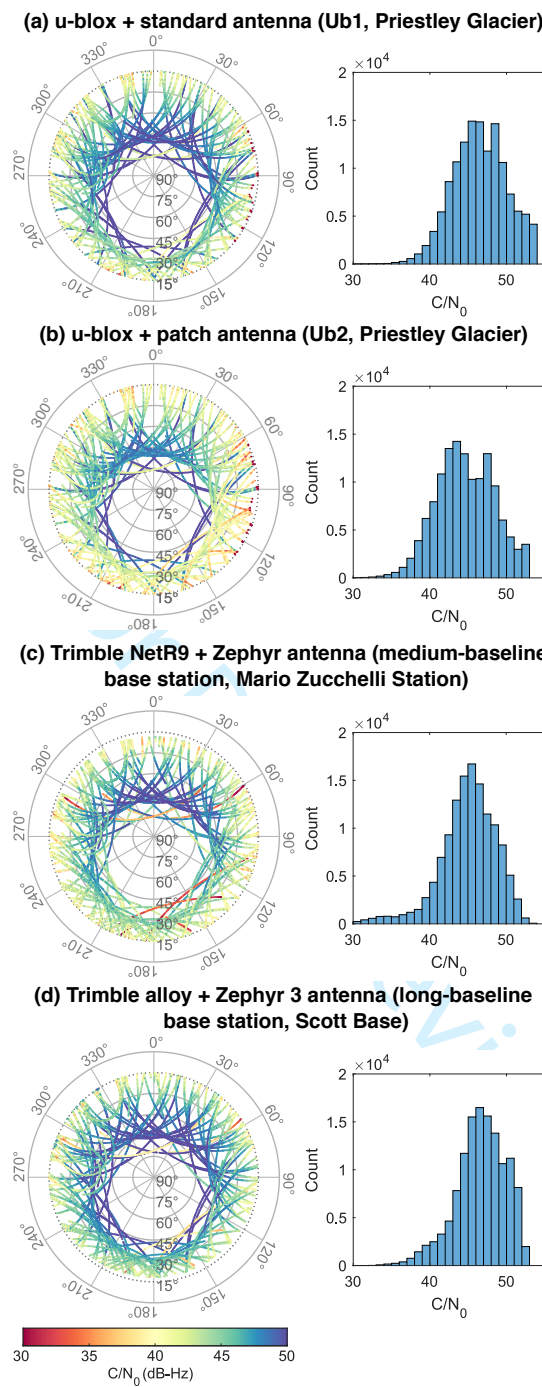


**Fig. 5.** Satellite skyplots with carrier-to-noise ( $C/N_0$ ) density ratios measured by each GNSS receiver. Satellite trajectories in each skyplot are shown for 12 hours on 21 November, 2022 with an elevation cutoff of  $15^\circ$ . All constellations are included (GPS L1, GLONASS L1, Galileo E1, Beidou B1, QZSS L1). The  $0^\circ$  azimuth corresponds to geographic north.

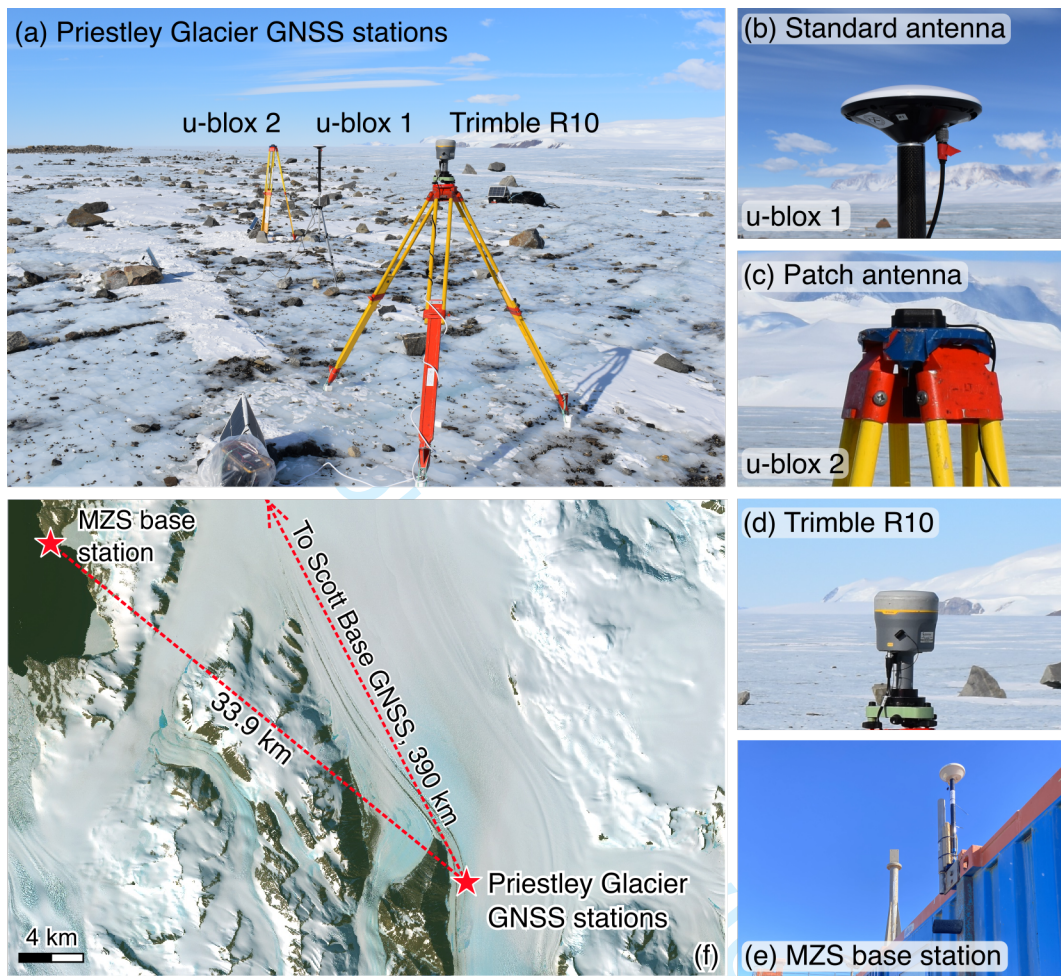


**Fig. 6.** Low-cost u-blox and survey-grade Trimble receivers and antennas installed on Priestley Glacier for 15 hours on 21 November, 2022 (Experiment 2). Panel (a) demonstrates the configuration of the roving receivers. Panels (b-d) show the antenna models compared in the experiment. Panel (e) demonstrates the set-up of the temporary base station installed at Mario Zucchelli Station (MZS). Panel (f) illustrates the configuration of the medium (33.9 km) and long (390 km) baselines in Experiment 2. The basemap in (f) is a Sentinel-2, 10 m true-colour image acquired on 18 December, 2022, courtesy of the European Space Agency.

237 was installed on the roof of a shipping container GNSS laboratory at Mario Zucchelli Station to support the medium  
238 baseline (33.9 km) test. This receiver tracked GPS, GLONASS, Galileo, Beidou, and QZSS satellite signals at 1 Hz  
239 (Fig. 6e). Existing reference stations in the Terra Nova Bay region do not record all available constellations and  
240 frequencies, and thus were unsuitable for this objective (Mario Zucchelli and Jang Bogo Station reference stations:  
241 both GPS and GLONASS only). The base station used for the long baseline test is the International GNSS Service  
242 (IGS) ground station established near Scott Base, 390 km southeast of Priestley Glacier (Johnston and others, 2017;  
243 LINZ, 2023). This receiver tracks GPS, GLONASS, Galileo, Beidou and QZSS satellite signals at a 10 second  
244 measurement interval.

#### 245 4.1 Medium-baseline positioning performance

246 Low-cost stations Ub1 (standard antenna) and Ub2 (patch antenna) provided millimetre-level precision (Fig. 7).  
247 Horizontal RMS<sub>2D</sub> errors were 8.4 mm and 9.7 mm for Ub1 and Ub2, respectively. The u-blox receivers were  
248 competitive with the Trimble system (RMS<sub>2D</sub> error: 8.3 mm), irrespective of choice of low-cost antenna (Table 4,  
249 Fig. 7). The almost identical performance of the low-cost and survey grade instruments is also shown by similarities  
250 in the derived ice velocity estimates. Based on only 12 hours of observations, ice velocities of  $100.3 \pm 0.5 \text{ ma}^{-1}$  (Ub1),  
251  $101.7 \pm 0.6 \text{ ma}^{-1}$  (Ub2),  $98.3 \pm 0.5 \text{ ma}^{-1}$  (Tr1) are estimated. No tidal vertical oscillation is observed because positions  
252 were recorded during the neap tide at a site near a glacier margin.

253 The vertical positioning error is approximately 3 to 4 times the horizontal error for both u-blox and Trimble  
254 observations from Priestley Glacier (Table 4, Fig. 7). The ratio between the vertical and horizontal error magnitude  
255 is closer to 2 at lower latitude sites (e.g., Yong and others, 2021; Hohensinn and others, 2022; Tidey and Odolinski,  
256 2023), due to a more favourable receiver–satellite geometry. While the total number of tracked satellites at the  
257 Priestley Glacier site is relatively high ( $n = 30$  to 32) and comparable to a mid-latitude site, the elevation angles  
258 of the satellites are lower at higher latitudes (Fig. 5). The geometry leads to a weaker vertical dilution of precision  
259 (VDOP), while the horizontal dilution of precision (HDOP) remains close to 1. A similar effect was also observed  
260 for the short baseline, stationary scenario (Experiment 1).

#### 261 4.2 Long-baseline positioning performance

262 All GNSS stations (Ub1, Ub2, Tr1) were capable of millimetre-level horizontal precision in a long baseline (390 km)  
263 configuration (Figs. 8 and 9). Low-cost station Ub1 paired with the standard antenna was competitive with the  
264 Trimble system (RMS horizontal errors were Ub1 = 6.2 mm and Tr1 = 6.5 mm). Of the three stations, the horizontal

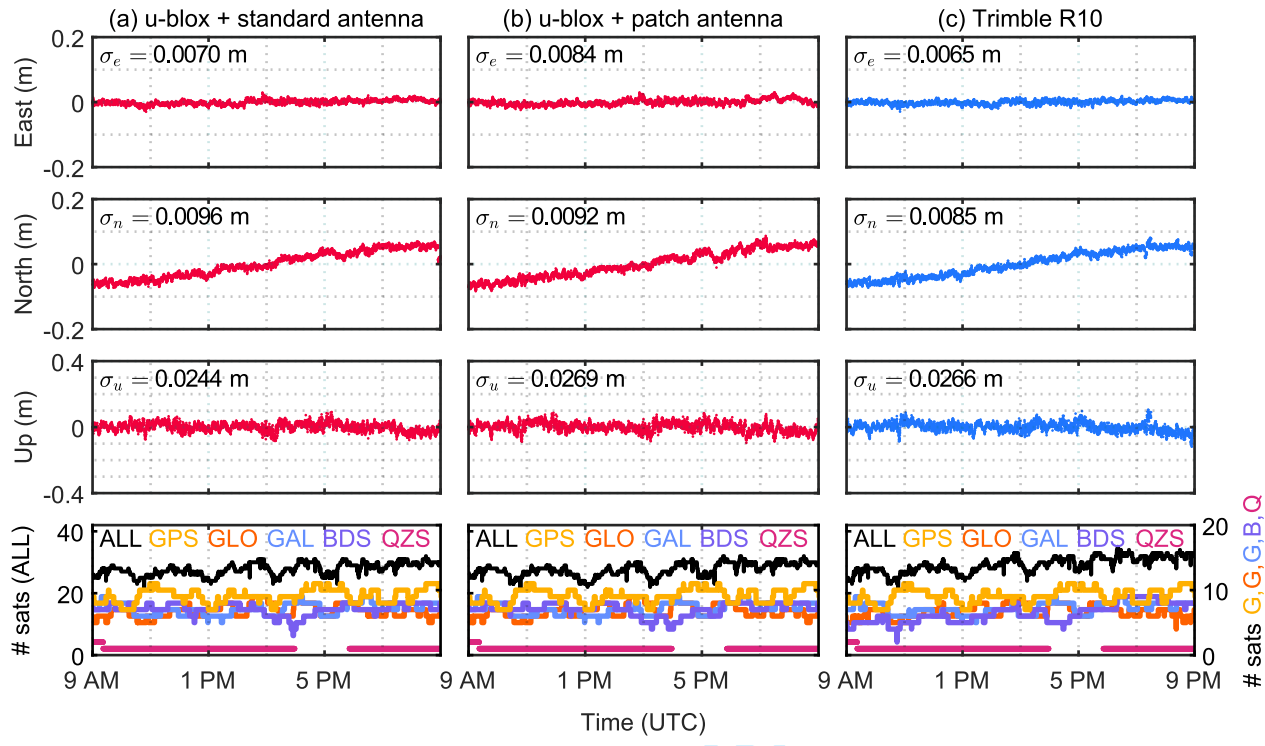


**Fig. 7.** Medium-baseline, dynamic positions recorded with u-blox and Trimble GNSS stations installed on Priestley Glacier for a 12 hour observation period on 21 November, 2022 (Experiment 2). East and north components of position correspond to the horizontal axes of the Antarctic Polar Stereographic coordinate system (EPSG:3031), with the mean position removed. Eastings and northing also correspond to local across-flow and along-flow directions, respectively (Fig. 1c). The baseline between the NetR9 base station and the on-glacier receivers is 33.9 km.  $\sigma_e$  and  $\sigma_u$  are standard deviations and  $\sigma_n$  is the standard deviation of the detrended northing component of position (i.e., displacement downstream).  $n = 4320$  epochs are included in each time series. Note the change in  $y$ -axis limits from  $\pm 0.2$  m for the horizontal components to  $\pm 0.4$  m for the vertical component.

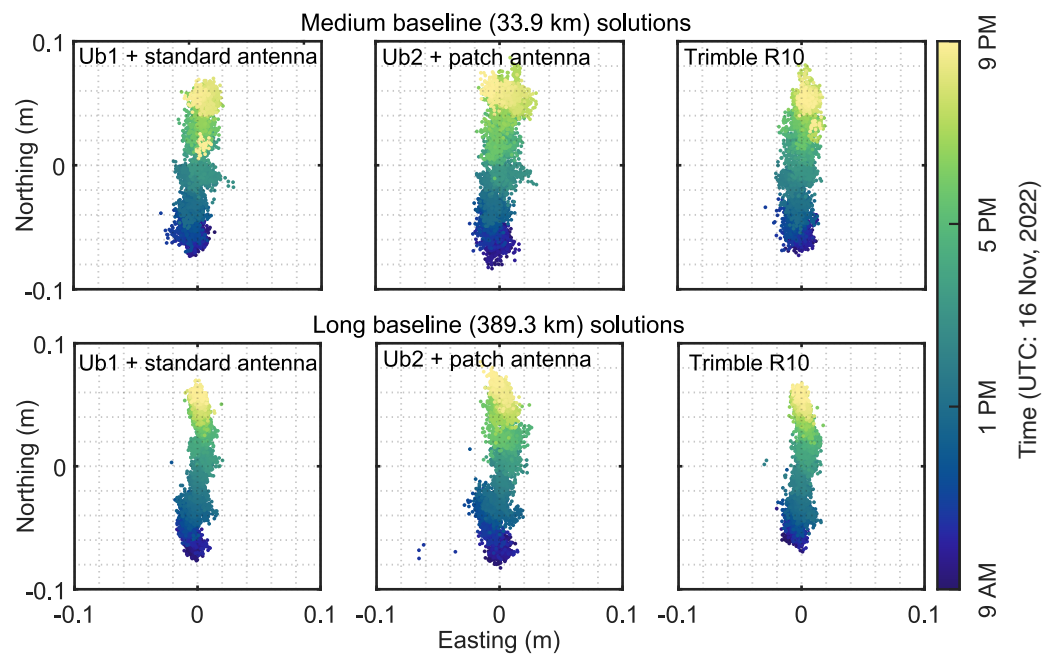


**Fig. 8.** Horizontal trajectories of the u-blox and Trimble GNSS stations installed alongside each other on Priestley Glacier for 12 hours on 21 November, 2022 (Experiment 2).  $n = 4320$  epochs are included in each solution.

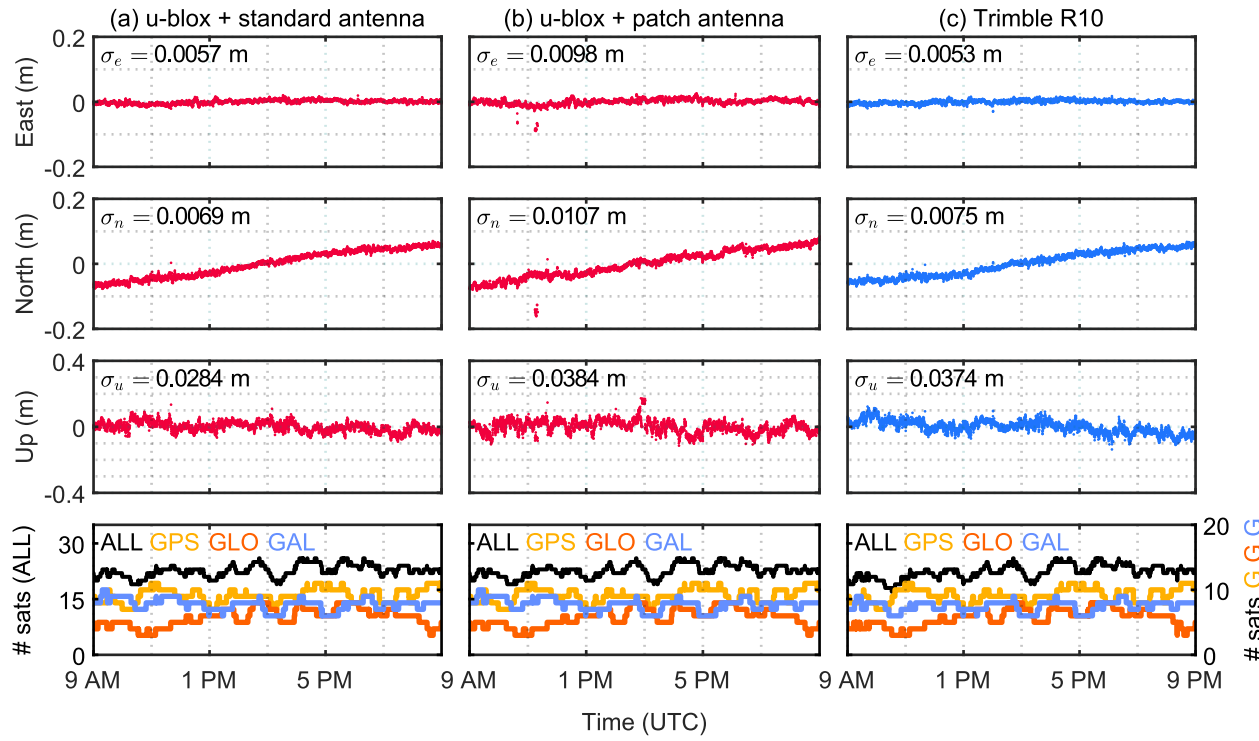


**Fig. 9.** Long-baseline, dynamic positions recorded with u-blox and Trimble GNSS stations installed on Priestley Glacier, for a 12-hour observation period on 21 November, 2022 (Experiment 2). The baseline between the Scott Base reference station and the on-glacier receivers is 390 km.  $\sigma_e$  and  $\sigma_u$  are standard deviations and  $\sigma_n$  is the standard deviation of the detrended northing component of position (displacement downstream).  $n = 4320$  epochs from a 12-hour observation period are included in each time series. Note the change in  $y$ -axis limits from  $\pm 0.2$  m for the horizontal components to  $\pm 0.4$  m for the vertical component.

and vertical positions acquired with the patch antenna were more susceptible to cycle slips and measurement noise (Fig. 9). All long baseline solutions presented here use three satellite constellations only (GPS+GLONASS+Galileo). Further improvements in long-baseline positioning performance are expected with the inclusion of Beidou and QZSS satellites (e.g., Odolinski and others, 2014; Odolinski and Teunissen, 2017).

Vertical positioning errors for all stations increased by approximately 30% in comparison to the medium baseline errors (Table 4). Conversely, the long-baseline configuration did not increase horizontal positioning errors despite the order of magnitude increase in baseline length. With all other error sources held equal, error magnitudes increase with increasing distance between base station and rover. We attribute the better-than-expected long-baseline results to the superior antenna hardware and siting of the Scott Base reference station (an IGS network station). The base station installed at Mario Zucchelli Station to support the medium baseline test was temporary, installed in a high-wind zone on top of a shipping container, paired with an early model Zephyr antenna of slightly inferior quality than the IGS station antenna (Zephyr 3, an antenna designed to significantly minimize multipath). Evidence of the difference in antenna hardware quality is shown by the distribution of the carrier-to-noise ( $C/N_0$ ) density ratios (a measure of signal strength, Fig. 5), where overall, observations from the Scott Base IGS station have higher  $C/N_0$  values than the Mario Zucchelli base station.

### 4.3 Multi-GNSS versus GPS positioning performance

This test compares multi-GNSS solutions (GPS, GLO, GAL, BDS, QZS) to single (GPS) and dual-GNSS (GPS and GLONASS) solutions from the medium-baseline (33.9 km) experiment conducted on Priestley Glacier. As expected, the five-constellation positioning solution yields smaller errors than the single (GPS) and dual-GNSS (GPS + GLONASS) solutions for both u-blox and Trimble systems (Fig. 10). Each multi-GNSS positioning solution includes at least twice as many tracked satellites in comparison to the single and dual-constellation solutions, leading to less measurement noise and a reduced frequency of undetected cycle slips that are characteristic of the single and dual-constellation solutions.

The low-cost u-blox system only achieves competitive performance to the Trimble system when three or more constellations are tracked. The Trimble system, however, provided centimetre-level precision for single (GPS) and dual (GPS + GLONASS) solutions, at epochs when the u-blox system experienced high signal noise and cycle slips (e.g., Fig. 10, epochs at 1000 UTC). One key advantage of the higher-cost Trimble system is therefore the ability to achieve precise positions and a stable time series unaffected by cycle slips when only GPS and GLONASS observations are available. We recommend that u-blox rover and base station pairs are configured to track at least

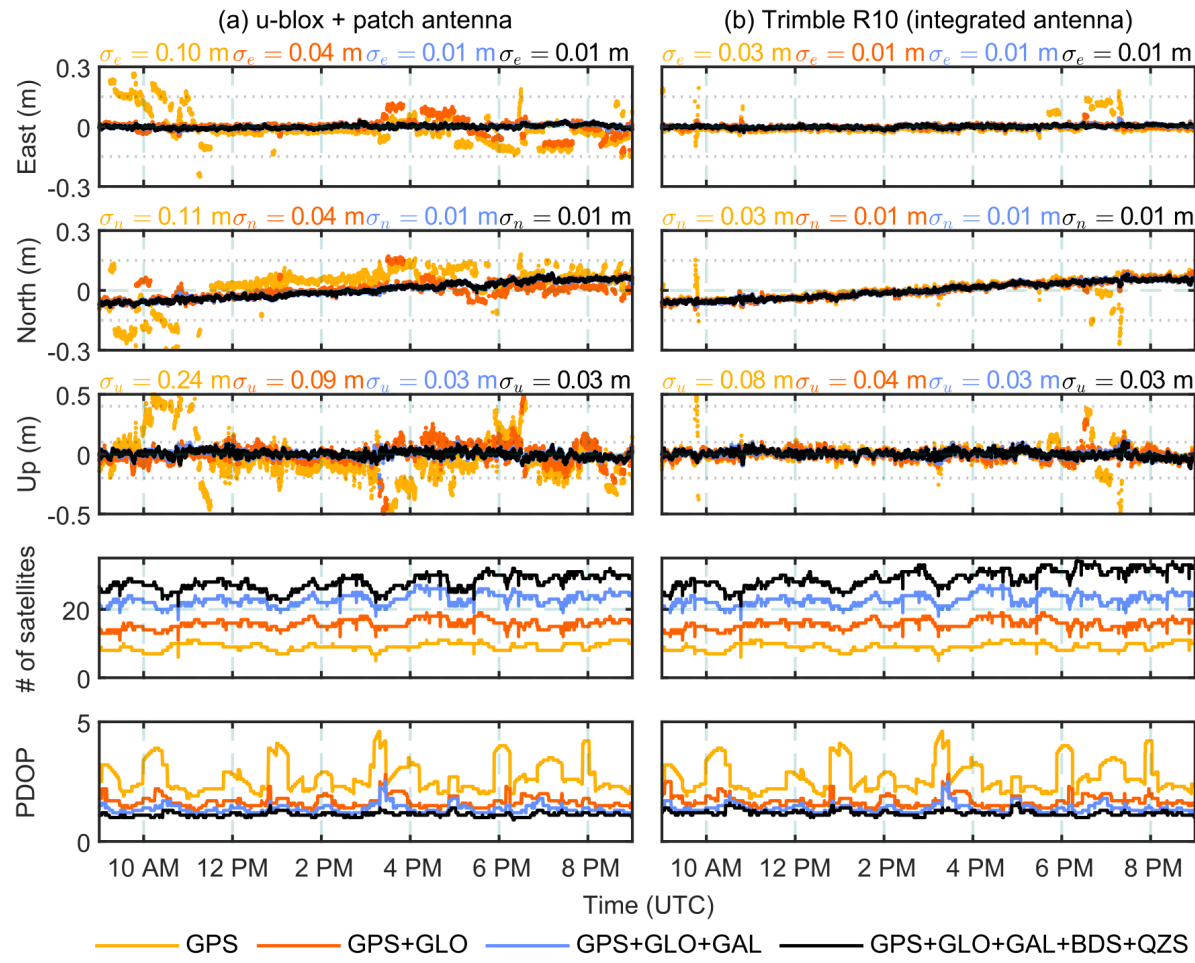


**Fig. 10.** East (across-flow), north (along-flow) and vertical (up) positioning solutions for two Priestley Glacier GNSS stations with the inclusion of additional satellite constellations. Each time series includes  $n = 4320$  epochs (10 s sample interval) collected over a 12-hour observation period on 21 November, 2022. The number of satellites is computed for an elevation cutoff angle of  $15^\circ$ . U-blox (a) and Trimble R10 (b) GNSS stations were installed as part of Experiment 2 (Fig. 6). Note the change in  $y$ -axis limits from  $\pm 0.3 \text{ m}$  for the horizontal components to  $\pm 0.5 \text{ m}$  for the vertical component.

294 GPS, GLONASS and Galileo satellites, at two or more frequencies, for successful low-cost GNSS positioning. To  
295 summarise, the dual-GNSS system (GPS+GLONASS) provided millimetre to centimetre-level precision when using  
296 a survey-grade receiver and antenna (Fig. 10), but may not suffice when using a low-cost GNSS system at this site.

#### 297 4.4 Low-cost antenna performance

298 The medium and long baseline experiments also evaluate the potential impact of different low-cost antenna types on  
299 the precision of the positioning results. For the long baseline, horizontal precision improved when the u-blox receiver  
300 Ub1 was paired with a multiband surveying antenna instead of a multiband patch antenna (RMS<sub>2D</sub> error for Ub1:  
301 6.2 mm vs. Ub2: 9.9 mm). Similarly, the standard antenna also improved the vertical precision for both medium  
302 and long baseline solutions (Table 4). Antenna type had no impact on horizontal error magnitudes in the medium  
303 baseline test.

304 The long baseline positions obtained with a patch antenna have larger error magnitudes because the simplified  
305 antenna hardware is more susceptible to signal noise (Fig. 5). Patch antennas do not contain internal shielding to  
306 mitigate multipath effects and cycle slips are also more frequent due to the antenna receiving a weaker, noisier signal  
307 (Fig. 9b). Raw signals received by the u-blox + patch antenna system have a lower  $C/N_0$  values overall, particularly  
308 for lower elevation satellites ( $<30^\circ$ ) (Fig. 5a-c). In other settings, low-cost patch antennas are also shown to have a  
309 lesser ability to suppress multipath interference and signal noise (Odolinski and Teunissen, 2017; Romero-Andrade  
310 and others, 2021; Paziewski, 2022; Manzini and others, 2022).

### 311 5 EXPERIMENT 3: MULTI-DAY GNSS RECORDS OF TIDALLY-MODULATED 312 ICE MOTION

313 Low-cost and survey-grade GNSS performance is evaluated in a realistic glacier monitoring scenario: observing  
314 tidally-modulated ice flexure across the floating shear margin of Priestley Glacier. At this site, ice velocities across  
315 the shear margin range from 0.1 to 0.3 m per day, and the amplitude of the tide-modulated vertical displacement is  
316 less than 5 cm (Still and others, 2022). This kinematic setting, characterised by small, centimetre-level displacements,  
317 creates a challenging environment from which to evaluate GNSS positioning performance. Multi-day records of glacier  
318 motion were observed at six GNSS stations (4 u-blox, 2 Trimble R10s) arranged in across- and along-flow transects  
319 (Fig. 1c). The across-flow transect began 600 m from the glacier margin because crevassing, meltwater ponding and  
320 frequent rockfalls prevented work nearer to the glacier margin. Trimble R10 station sites were selected to measure  
321 ice velocity at the recent (November 2022) and original (January 2020) locations of a shallow-ice core drilling site

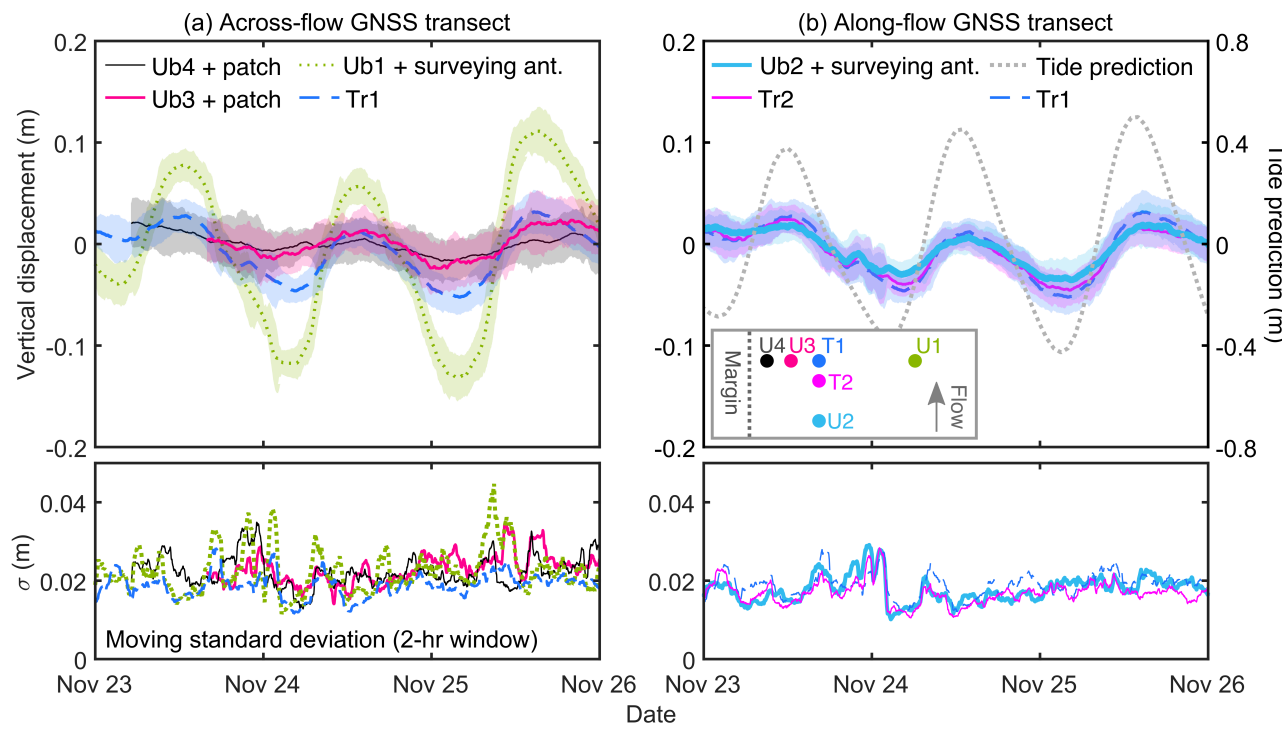


**Fig. 11.** The tide-modulated vertical displacement of four u-blox and two Trimble GNSS stations on Priestley Glacier. Panel (a) includes the stations installed in an across-flow transect. Panel (b) includes the stations installed in an along-flow transect, and a tide prediction from the CATS2008 model (Padman and others, 2002; Howard and others, 2019). Shaded error bounds show the moving standard deviation (two-hourly window) of the vertical position time series. These GNSS stations are expected to exhibit vertical oscillations with varying amplitudes due to their different locations with respect to the glacier margin and grounding zone. GNSS station locations are mapped in Fig. 1c.

322 (Thomas and others, 2021; Lutz and others, 2022).

323 Horizontal and vertical displacement of the ice surface was observed at a 1-second sampling interval for 3 to 9 days,  
 324 depending on science priorities. Kinematic positions from the on-glacier GNSS stations are processed with respect  
 325 to the temporary base station installed at Mario Zucchelli Station (33.9 km baseline). We present six GNSS time  
 326 series of tidally-modulated across- and along-flow ice displacement and velocity with estimated positioning errors. In  
 327 this experiment, it is expected that amplitudes of the E/N/U position time series for each station will vary due to  
 328 the different receiver locations with respect to the glacier margin, while the timing of high and low tide peaks should  
 329 be synchronised.

### 330 5.1 Vertical ice motion

331 This experiment examines the sensitivity of the different receiver and antenna configurations in detecting short  
332 time-scale observations in a kinematic setting. Vertical ice motion at a predominantly solar diurnal tidal frequency  
333 is observed at all GNSS sites (Fig. 11). Focusing on the low-cost configurations, stations Ub4 (600 m from the  
334 margin) and Ub3 (800 m from the margin), detected clear diurnal tidal oscillations with amplitudes less than 1 and  
335 2 cm, respectively (Fig. 11a), in good agreement with the timing of the CATS2008 tide prediction (Padman and  
336 others, 2002; Howard and others, 2019). Predicted tidal amplitudes and GNSS-observed amplitudes differ because  
337 the Priestley Glacier field site is near the edge of the CATS2008 model domain, in a relatively narrow fjord and thus  
338 is not freely-floating in hydrostatic equilibrium.

339 The survey-grade and low-cost systems again perform similarly in this dynamic setting (Table 4). Vertical  
340 positions recorded by the three GNSS stations in the along-flow transect (Fig. 11b) have very similar signal amplitudes  
341 and error magnitudes, irrespective of receiver or antenna type. Similar uncertainties are achieved in all of the GNSS  
342 configurations reported here (Fig. 11, Table 4). For example, the average of the moving standard deviation  $\sigma_u$ , a  
343 measure of observation noise associated with vertical positioning, is 4.3 cm (Ub3) and 4.0 cm (Ub4) for the u-blox  
344 + patch antenna configurations, and 3.8 cm (Ub1) and 3.7 cm (Ub2) when standard surveying antennas are used.  
345 Three explanations for marginally smaller vertical errors derived from stations Ub1 and Ub2 are firstly the more  
346 advantageous satellite–receiver geometry – the receivers were installed a greater distance from Black Ridge and have  
347 an unobstructed skyview (Fig. 1c). Ub1 and Ub2 were also able to track an additional 1 to 2 satellites at each epoch  
348 and thirdly were paired with low-cost surveying antennas rather than patch antennas.

### 349 5.2 Horizontal ice motion

350 Tidally-modulated along- and across-flow ice displacement is observed at all GNSS stations (Fig. 12). All u-blox and  
351 Trimble stations operated with a precision that allowed the detection of velocity variability at a diurnal frequency  
352 (Fig. 12). In the along-flow direction, ice velocity increases during the falling tide, and slows during the rising tide,  
353 with one velocity maximum observed per diurnal tide cycle. In the across-flow direction, the observed transverse  
354 displacement of ice (towards and away from the margin) is associated with elastic bending. On the rising tide, ice  
355 is displaced toward the margin and on the falling tide ice is displaced toward the glacier centre (Fig. 12). The  
356 amplitude of these oscillations ranges from ±1.5 cm (Ub4, nearest the glacier margin) to ±3 cm (Ub1,  
357 nearest the glacier centre).

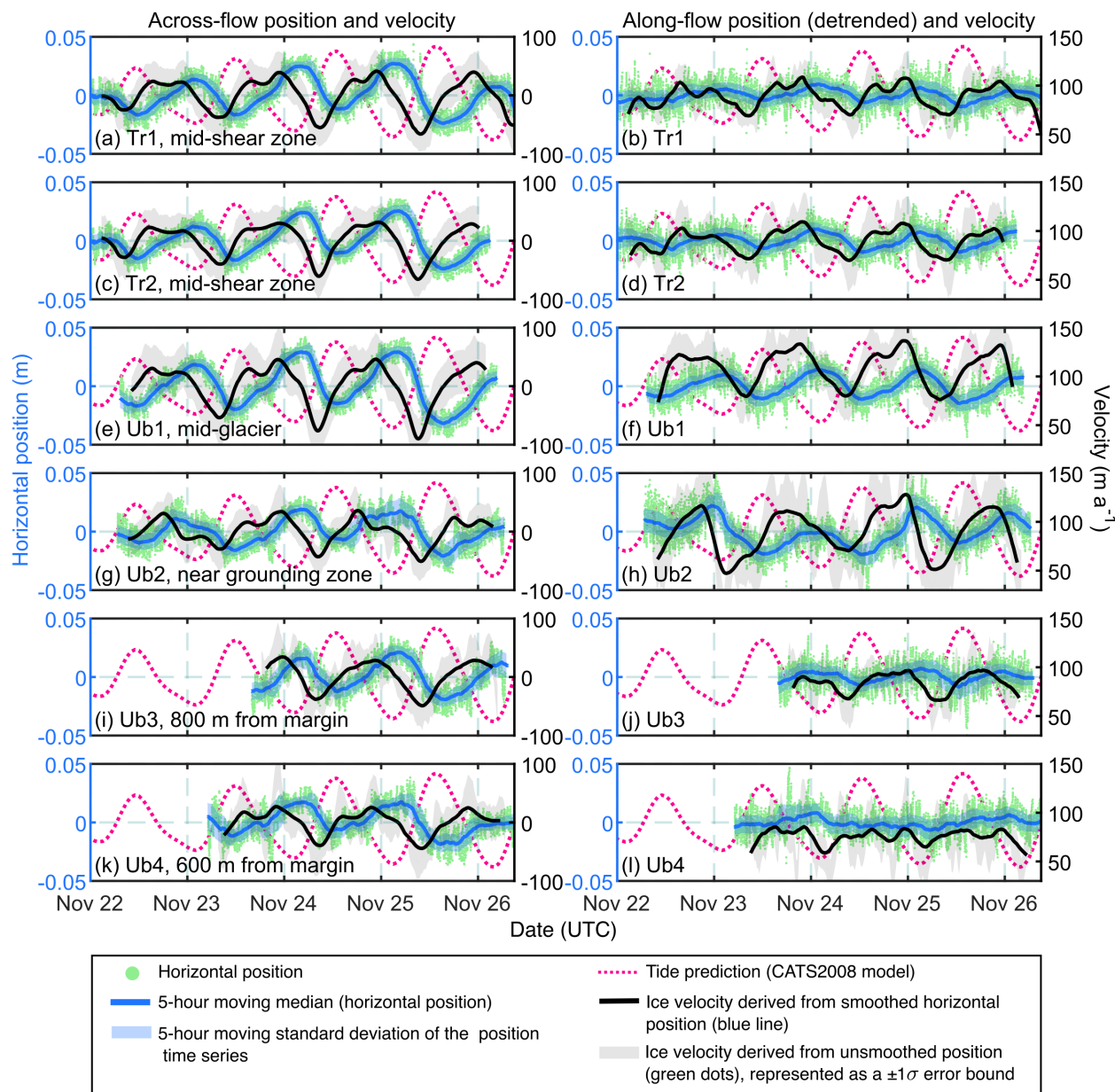


**Fig. 12.** Across and along-flow ice displacement and velocity at each Priestley Glacier GNSS station. GNSS positions (green dots) are smoothed with a five-hour moving median filter (dark blue line). Shaded blue error bounds represent  $\pm 1\sigma$  in horizontal position over a five-hour sliding window. In column 1, across-flow displacement in the negative (positive) direction indicates motion toward (away from) the glacier margin. In column 2, the along-flow displacement is presented with the mean linear flow removed. Along-flow displacement in the positive direction indicates an increased downstream flow rate. The ice velocity (black line) is a linear least-squares fit between the smoothed displacement (blue line) and time. The grey error band denotes the velocity computed from unsmoothed positions (green dots), presented as a  $\pm 1\sigma$  error band. The tide prediction is from the CATS2008 model (Padman and others, 2002; Howard and others, 2019). Neap tide occurred on the 20 November, 2022.

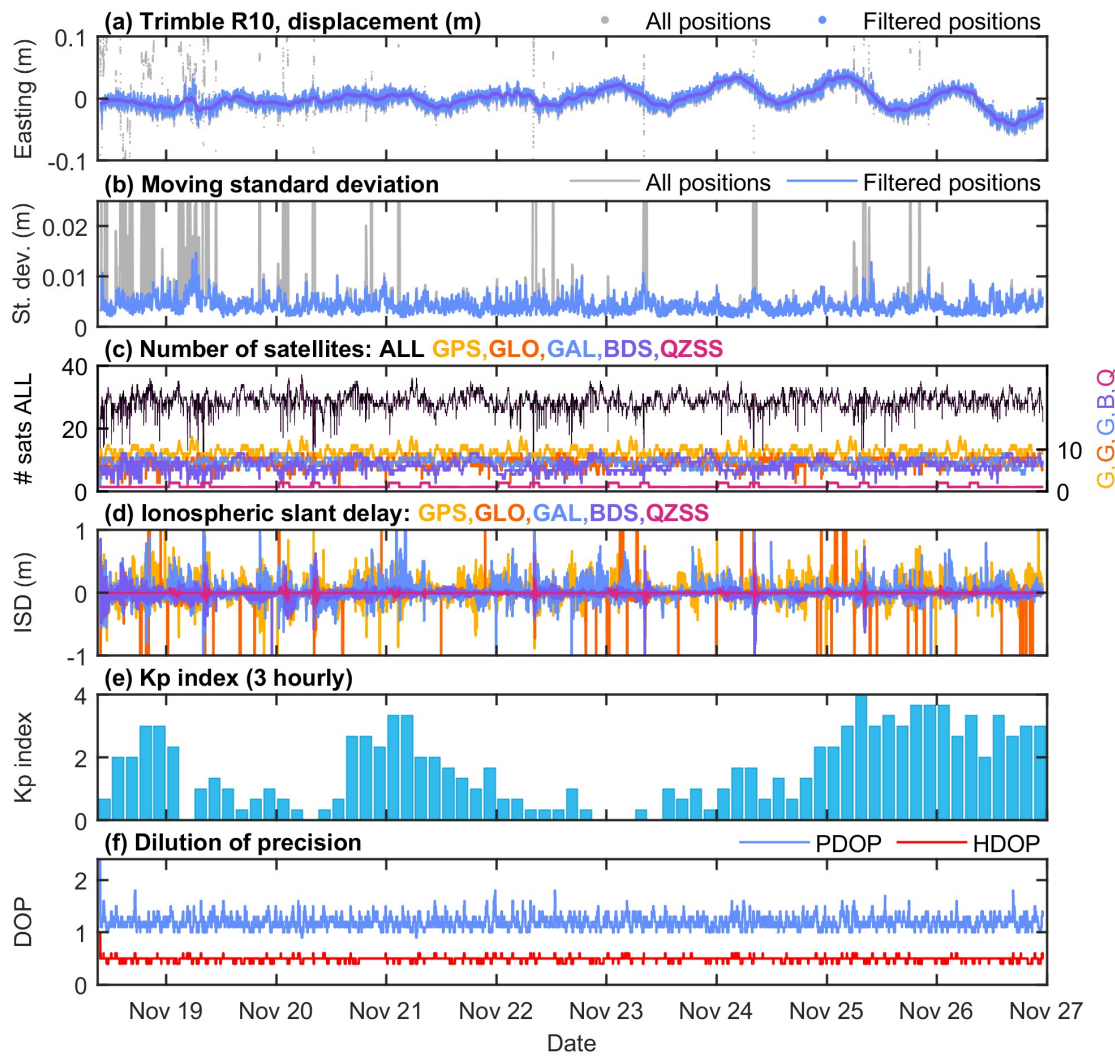


**Fig. 13.** The association between positioning noise, satellite–receiver geometry and ionospheric conditions at station Tr1. Panel (a) shows the easting component of position. Filtered position time series have outliers removed as described in Section 2.2. Panel (b) shows the corresponding moving standard deviation, computed for 1-hourly windows (360 epochs). Panel (c) shows the number of satellites tracked at each epoch. Panels (d) and (e) show the slant ionospheric delay and the Kp index (NOAA, 2023), a measure of global ionospheric disturbance. Panel (f) shows the variability in the horizontal dilution of position (HDOP) and positional 3D dilution of precision (PDOP). In this analysis, only the easting component of horizontal position is presented for brevity. Similar conclusions are drawn from time series of the northing and vertical components of position.

### 358 5.3 Sources of positioning error

359 In this section, we consider the causes of positioning errors at the Priestley Glacier field site. Variability in positioning  
360 noise is shown by the moving standard deviation computed for each position time series (Fig. 11b). Peaks and  
361 trends in the moving standard deviations are synchronised between all six of the GNSS stations, despite their  
362 different locations across the glacier shear margin. This consistency across GNSS stations indicates that variability  
363 in positioning noise is not predominately due to site specific multipath interference effects or differences in hardware  
364 (low-cost versus survey-grade receivers, or standard versus patch antennas). Instead, the number of tracked satellites,  
365 or the similarities in ionospheric and tropospheric conditions, may determine the magnitude of positioning errors at  
366 the Priestley Glacier site.

367 Time-varying satellite geometry and atmospheric effects are demonstrated using the longest duration position  
368 time series from station Tr1 (Trimble R10, 10-day duration, Fig. 13). Short-term increases in positioning noise  
369 coincide with rapid decreases in the number of tracked positioning satellites (e.g., the epochs at 0800 hours on  
370 November 19 in Fig. 13e). The HDOP and PDOP, however, remain steady over the ten-day measurement period  
371 due the high number of positioning satellites tracked at all epochs (Fig. 13f). A second source of error, the prevailing  
372 ionospheric conditions (indicated by the K<sub>p</sub> index) has no apparent association with observed positioning noise  
373 (Fig. 13). Similarly, large variations in the slant ionospheric delay time series, defined as the estimated delay as  
374 the GNSS signal passes through the ionosphere, have very little association with positioning error magnitudes. This  
375 result indicates that the ionospheric estimation modelling strategy used (Table 3) correctly estimates the ionospheric  
376 delays, and therefore has very little effect on positioning errors. Priestley Glacier GNSS datasets were collected  
377 during a period of low to medium ionospheric disturbance (K<sub>p</sub> index  $\leq 4$ ) and a longer time series encompassing a  
378 wider range of geomagnetic disturbances is required to further investigate these effects.

## 379 6 DISCUSSION

380 GNSS positioning performance at high latitude sites may be affected by relatively low satellite elevations, which result  
381 in weaker receiver–satellite geometries and longer signal paths through the ionosphere. Nonetheless, the positioning  
382 performance of u-blox GNSS stations at our high-latitude glacier site is similar to performance evaluations of the same  
383 equipment at mid-latitude sites. For example, kinematic positioning evaluations of u-blox receivers have reported  
384 horizontal precision of  $\sigma_e$  and  $\sigma_n = 10$  mm (Odolinski and Teunissen, 2020) (RTK, long baseline: 112 km) and  
385  $\sigma_e = 8$  and  $\sigma_n = 10$  mm (Tidey and Odolinski, 2023) (RTK, medium baseline: 27 km). In the present experiments,

386 equivalent data processing approaches applied to low-cost and survey-grade observations resulted in comparable RMS  
387 errors for each baseline length (Table 4). The high-cost, survey-grade system offered no performance advantages. At  
388 longer baselines, pairing the low-cost receiver with a ground-plane surveying antenna (rather than a patch antenna)  
389 resulted in a small improvement in precision.

### 390 6.1 Set-up of low-cost systems for successful precise positioning

391 The u-blox ZED-F9P receivers used here have the capability to track multi-GNSS dual-frequency signals (e.g., GPS  
392 and GLONASS: L1 and L2, Galileo: E1 and E5b). Dual-frequency observations enable medium and long baseline  
393 positioning with low-cost systems (Odolinski and Teunissen, 2020). The GNSS signal is delayed as it travels through  
394 the ionosphere, and this effect is amplified as baseline length increases and satellite elevation decreases, leading to  
395 errors on the order of tens of metres (Odijk and Wanninger, 2017). Estimation of the ionospheric delay is therefore  
396 necessary for medium and long baselines, but can be neglected for a shorter baselines, in which case the delays are  
397 approximately equal. Dual-frequency data can be used to estimate slant ionospheric delays, leading to more precise  
398 estimates and improved ambiguity resolution performance (Odolinski and Teunissen, 2020). In the present work,  
399 centimetre-level precision over a long baseline (390 km) is achieved in this way. Single-frequency low-cost modules  
400 will not achieve comparable results. Multi-GNSS solutions (i.e., GPS + GLONASS + Galileo + Beidou + QZSS)  
401 provide an improved satellite geometry and redundancy in observations, leading to improvements in precision (e.g.,  
402 Odolinski and others, 2015a; Paziewski and Wielgosz, 2017; Xue and others, 2021).

403 Single-constellation and dual-constellation solutions are widely used for GNSS positioning in Antarctica, partic-  
404 ularly when employing precise point positioning (PPP) services such as the CSRS-PPP service (Banville and others,  
405 2021), or when applying corrections from permanent long-term reference stations for kinematic positioning. In the  
406 latter case, existing GNSS reference stations in Antarctica are often configured to receive GPS and GLONASS sig-  
407 nals only. For example, the nearby Mario Zucchelli and Jang Bogo Station reference GNSS stations in Terra Nova  
408 Bay both recorded GPS and GLONASS signals only during our field campaign. Installation of a temporary base  
409 station on stationary ground to track additional constellations may be beneficial for low-cost kinematic positioning  
410 if millimetre- to centimetre-level precision is required. The multi-GNSS solutions presented here outperformed the  
411 single or dual-constellation solutions for both low-cost and survey-grade receivers (Fig. 10).

412 The precision and accuracy of GNSS positions can be improved by pairing the low-cost receivers with survey-  
413 grade or geodetic antennas (e.g., Odolinski and Teunissen, 2017; Krietemeyer and others, 2020; Romero-Andrade  
414 and others, 2021). Performance improvements associated with the use of geodetic or survey-grade antennas are

well established and we do not evaluate this further here. Instead, we compared the performance of low-cost patch antennas and low-cost standard surveying antennas to meet the objective of using a purely low-cost system. In cases where sub-centimetre precision is required, or when working with long baselines exceeding 100 km, using a low-cost surveying antenna rather than a patch antenna may lead to improved precision (e.g., Table 4). In the long baseline (390 km) test (Experiment 2), we observed a 30% reduction in the 3D RMS error when using a low-cost surveying antenna instead of a patch antenna.

## 6.2 Processing low-cost data: kinematic single-baseline positioning versus PPP strategies

The present work focuses on single-baseline kinematic positioning (a relative positioning method) because it can provide the millimetre- to centimetre-level precision required for glaciological applications. Error magnitudes are a function of baseline length, with millimetre-level precision anticipated for short baselines (<20 km), however, the common notion that a base station must be located within a few tens of kilometres is not necessarily a requirement, particularly for dual-frequency, multi-GNSS observations. Centimetre-level precision is feasible over long baselines >100 km (Fig. 9, Schüler, 2006; Odolinski and Teunissen, 2020), and indeed, the present work achieved centimetre-level precision for both low-cost and survey-grade systems with a 390 km baseline (Fig. 9).

PPP, a single-receiver positioning method, is often used in Antarctica. The approach is convenient for locations far from a reference station or without access to a stationary reference point. Precise positioning can be achieved with PPP (Kouba and others, 2017), however, these solutions are limited by proximity of the receiver to the network of reference stations from which orbit and clock correction products are derived (Geng and others, 2010). PPP convergence times are much longer than for relative positioning when corrections for atmospheric delays are absent. PPP solutions are also highly sensitive to ionospheric conditions and the quality of precise orbit and clock correction products.

Comparisons between single-baseline kinematic positioning solutions and PPP solutions are presented in Fig. 14. Stationary time series (Fig. 14a) were recorded by the u-blox and Trimble R10 systems installed at Mario Zucchelli Station for Experiment 1. These observations are processed in kinematic mode, that is, the same parameter settings used for dynamic observations from a glacier. The correct solution for the stationary time series is zero displacement with time, and therefore, any excursions from zero displacement quantify the PPP solution quality. We evaluate the PPP solution generated by the online CSRS-PPP service (GPS+GLONASS only) and an alternative RTKLIB PPP solution (GPS + GLONASS + Galileo). The CSRS-PPP and RTKLIB-PPP solutions fluctuate over hourly timescales

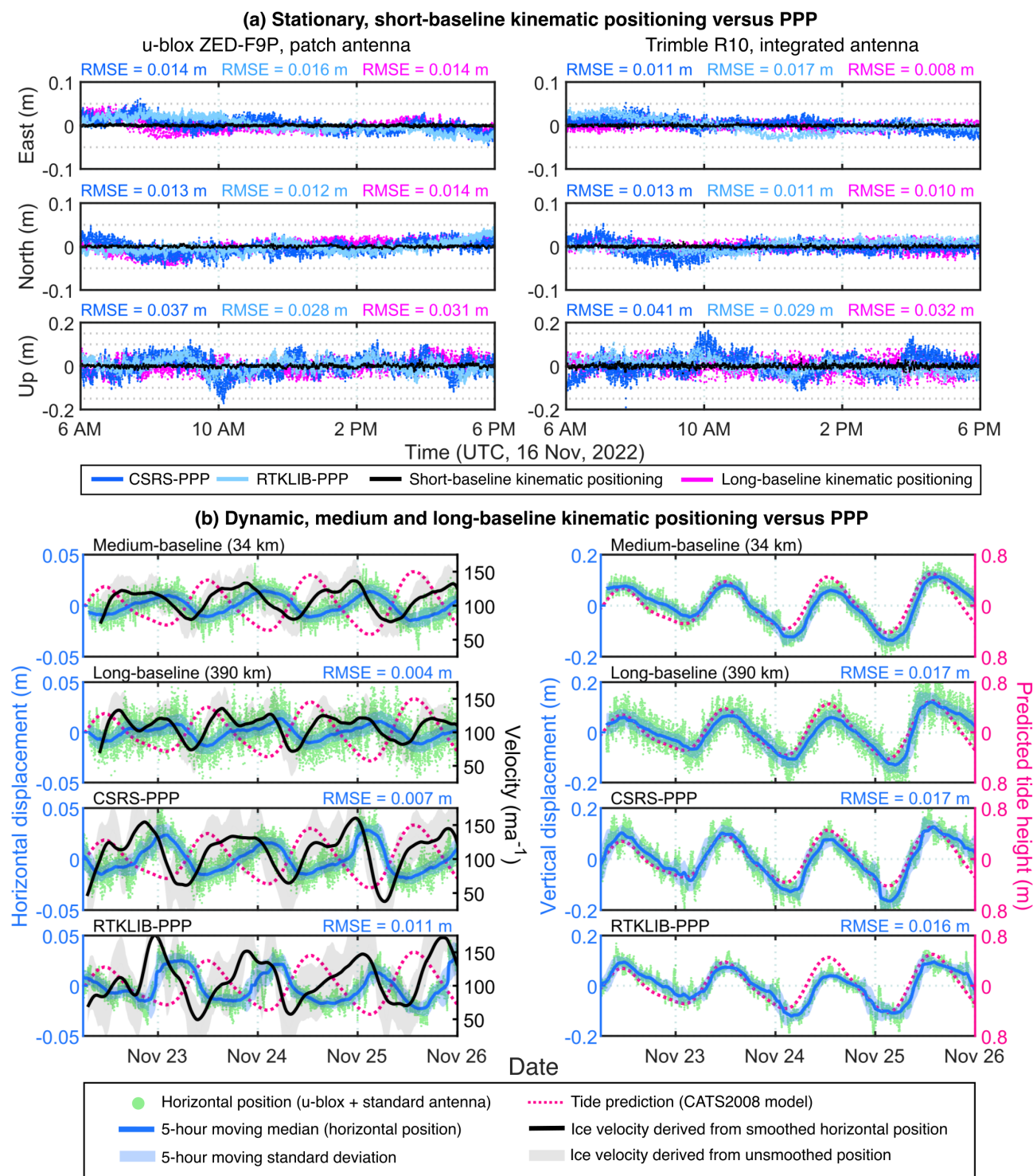


**Fig. 14.** Comparisons between single-baseline kinematic positioning and precise point positioning (PPP) solutions. The time series in (a) contain stationary u-blox and Trimble R10 observations from Experiment 1. Root mean square error (RMSE) values describe the difference between the expected position (zero displacement with time) and the observed positions. The time series in (b) contain dynamic observations from low-cost station Ub1 installed on Priestley Glacier (Experiment 3). RMSE values describe the difference between the expected displacement (the medium-baseline solution) and alternative solutions (long-baseline, CSRS-PPP and RTKLIB-PPP solutions).

444 in a manner not clearly attributable to any physical process (Fig. 14a). These errors are not a limitation when tracking  
445 decimetre-level displacements, but could lead to erroneous interpretations of short-duration observations, or when  
446 measuring small deformations (propagated errors on velocity and strain rates are magnified) (e.g., Fig. 14b). Choosing  
447 low-cost u-blox hardware instead of survey-grade hardware will not degrade the precision of the PPP solution.

448 Single-baseline and PPP solutions for dynamic positioning are compared using data from station Ub1 installed  
449 on Priestley Glacier (Exp. 3; Fig. 14b). For this comparison, we take the medium-baseline solution as the expected  
450 solution. The RMS error is used to compare alternative positioning solutions to the expected solution. Long-baseline  
451 positioning (390 km, GPS+GLONASS+Galileo) provided better horizontal positioning performance in terms of RMS  
452 errors than the CSRS-PPP (GPS+GLONASS) and RTKLIB-PPP (GPS+GLONASS+Galileo) solutions (Exp. 3;  
453 Fig. 14b). CSRS and RTKLIB-PPP positioning solutions were again affected by erroneous excursions that led to  
454 inconsistent estimates of the diurnal variation in ice velocity.

### 455 6.3 Applications and advantages of low-cost positioning in Antarctica

456 The low-cost positioning systems installed on Priestley Glacier consumed approximately half as much power as the  
457 survey-grade systems (Table 2). Power usage depends on the choice of both receiver, data logger, and antenna  
458 hardware (amplified surveying multiband antenna models consume more power than patch antenna models), and  
459 the observation sampling frequency. Low-cost positioning systems used in the present work logged all available  
460 constellations at a 1 Hz frequency while supported by a pair of small 12 V solar panels (28 cm × 28 cm) and a  
461 single 18 A h SLA battery. Further development and testing of GNSS stations with relatively low power usage is an  
462 important objective because continuous GNSS records of polar ice dynamics are biased toward the summer months  
463 (e.g., Greene and others, 2020; Klein and others, 2020), with data gaps arising from difficulties in maintaining a  
464 steady power supply during the darkness of the polar winter (Jones and others, 2016). Low-cost GNSS stations, such  
465 as the dual-frequency u-blox F9P units tested here, can support longer duration, potentially continuous year-round,  
466 monitoring in remote environments where power requirements are logistically challenging.

467 Installation of a temporary low-cost base station to support a field campaign is possible without significant  
468 cost barriers. Where centimetre-level rather than decimetre-level precision is required, a low-cost, single-baseline  
469 solution may yield positions with better precision and accuracy than a PPP solution (Fig. 14). With dual-frequency  
470 receivers and multi-GNSS configurations such as the five-system (GPS+GLO+GAL+BDS+QZS) configuration used  
471 in the present work, medium- to long-baseline kinematic positioning (>300 km) is feasible (Experiment 2) and may  
472 provide improved precision and accuracy over PPP (Fig. 14). Long-baseline positioning solutions can also provide

473 redundancy and quality control when relying on PPP solutions.

474 The precision of the positioning system determines the smallest measurable ice displacement or change in velocity.  
475 The low-cost GNSS units tested on Priestley Glacier operated with centimetre-level horizontal and vertical precision,  
476 suitable for a range of glaciological applications. Minimum horizontal and vertical tidal oscillations detected by  
477 the low-cost systems were  $\sim 1$  cm and  $\sim 1.5$  cm, respectively (Figs. 11 and 12). The precision of the low-cost  
478 units is suitable for the observation of tide-modulated ice motion velocity gradients within a single week-long field  
479 campaign, with no return to the site required. Nearer to the glacier margin, where ice displacement approaches zero,  
480 measurement noise begins to exceed the amplitude of displacement, although the mean position is well defined and tide  
481 signals are still detectable. At field sites such as the Ross Ice Shelf, where the tidal range is approximately 3 m and ice  
482 velocities exceed  $600 \text{ m a}^{-1}$  (Brunt and others, 2010; Klein and others, 2020), low-cost systems are more than adequate  
483 for detecting such large displacements. Low-cost GNSS units similar to the set-ups evaluated here are also suitable for  
484 densifying existing GNSS monitoring networks or reference stations. For single-season, temporary occupations of field  
485 sites, the significantly lower cost combined with lesser power consumption motivates the deployment of additional  
486 GNSS stations for improved spatial coverage and repeatability for studies of ice kinematics and mechanics.

## 487 7 CONCLUSIONS

488 Low-cost, mass-market dual-frequency GNSS receivers are capable of precise and reliable positioning at high-latitude,  
489 glaciated sites, with errors comparable to high-cost systems. This result was obtained by comparing horizontal and  
490 vertical positions from co-located u-blox ZED-F9P GNSS receivers ( $<\$300$  USD) and survey-grade Trimble R10  
491 receivers ( $\sim \$10,000$  USD second-hand,  $>\$30,000$  USD new) under stationary and dynamic conditions in Terra Nova  
492 Bay, Antarctica. RMS horizontal errors (Table 4) indicate almost identical performance for short baselines (u-blox  
493 + patch antenna: 2 mm, Trimble: 2 mm), medium baselines (u-blox + surveying antenna: 8 mm, Trimble: 8 mm)  
494 and long baselines (u-blox + surveying antenna: 6 mm, Trimble: 7 mm). A low-cost ground-plane surveying antenna  
495 provides a slight advantage over a patch antenna at longer baseline lengths.

496 We installed four low-cost GNSS stations and two survey-grade stations on Priestley Glacier to evaluate the  
497 performance and reliability of each system in a challenging kinematic setting characterised by centimetre-level ice  
498 displacements. The efficacy of low-cost GNSS depends on the magnitude of the observation noise, relative to the  
499 signal of interest. Multi-day time series of 3D ice motion show that the low-cost systems operated with a level of  
500 precision useful for measuring tide-modulated velocity variability at semidiurnal and diurnal frequencies, at a field  
501 site where vertical ice displacement is  $<5\text{cm}$  per day, and horizontal ice motion  $<20\text{ cm}$  per day. A low-cost GNSS

502 station installed within 600 m of glacier margin detected tidal horizontal oscillations of  $\pm 1$  cm. Such high-precision  
503 results will be reproducible in other study sites in Antarctica, providing that dual-frequency, multi-constellation  
504 receiver and antenna hardware is used.

505 Successful positioning with the u-blox system is possible with both single-baseline kinematic positioning, which  
506 requires a rover and base station receiver pair, and single-receiver precise point positioning (PPP). While we use  
507 kinematic positioning due to its inherently smaller error magnitudes at short to medium baselines, remote field settings  
508 may necessitate the application of PPP techniques. Focusing on PPP methods alone, the positioning precision of  
509 low-cost PPP solutions were again comparable with survey-grade solutions (Fig. 14) generated with the open-  
510 source RTKLIB software (Takasu and Yasuda, 2009) and the online CSRS-PPP service (Banville and others, 2021).  
511 Although we recommend single-baseline kinematic positioning when observing small centimetre-level displacements  
512 (and detecting variability in derived velocity), the choice of a low-cost rather than survey-grade hardware did not  
513 compromise positioning performance when using PPP.

514 The experiments presented here provide a ‘proof of concept’ of the efficacy of low-cost GNSS positioning systems  
515 for glaciological monitoring applications. The mass-market receivers and antennas evaluated here yield both a con-  
516 siderable cost advantage and a reduction in power consumption in comparison to a survey-grade system. The results  
517 of these experiments encourage the widespread use of low-cost receivers to expand and densify GNSS monitoring  
518 networks, both in Antarctica and in glaciated regions worldwide.

## 519 8 DATA AND SOFTWARE

520 The long baseline positioning uses multi-GNSS observations from the International GNSS Service (IGS) station  
521 SCTB near Scott Base, maintained by LINZ (2023) and downloaded in RINEX 3 format from the European Space  
522 Agency (ESA) GNSS Science Support Centre: <https://gssc.esa.int/>. Daily multi-GNSS broadcast ephemeris files  
523 (BRDM00DLR product) (Steigenberger and Montenbruck, 2020) are from the CDDIS GNSS data archive (Noll,  
524 2010): [https://cddis.nasa.gov/Data\\_and\\_Derived\\_Products/GNSS/gnss\\_mgex.html](https://cddis.nasa.gov/Data_and_Derived_Products/GNSS/gnss_mgex.html). Final multi-GNSS precise  
525 orbit and clock information (Deng and others, 2016; Montenbruck and others, 2017) generated by the GFZ Anal-  
526 ysis Centre are available from the Analysis Center of the Multi-GNSS Experiment (MGEX): <https://www.gfz-potsdam.de/en/section/space-geodetic-techniques/projects/mgex>. Global K<sub>p</sub> index values (Matzka and others, 2021)  
527 presented in Fig. 13 were downloaded from <https://kp.gfz-potsdam.de/en/data>. Modified Sentinel-2 images in Fig. 1  
528 were downloaded from <https://scihub.copernicus.eu/dhus/#/home>.

529 The software u-center v22.07 is available at <https://www.u-blox.com/en/product/u-center>. The Trimble RINEX

531 Converter ‘ConvertToRINEX v3.14.0’ software is available at <https://geospatial.trimble.com/trimble-rinex-converter>.  
532 Hatanaka-compressed RINEX files are uncompressed with the RNXCMP software available at: <https://terras.gsi.go.jp/ja/crx2rnx.html>. GNSS datasets were processed with the open-source software RTKLIB (v.2.4.3 b34, developed by  
533 T. Takasu, Takasu and Yasuda (2009)), available at <https://rtklib.com/>. CSRS-PPP solutions (Banville and others,  
534 2021) were generated with the online service: <https://webapp.csrs-scrs.nrcan.gc.ca/geod/tools-outils/ppp.php>.  
535 The CATS2008 tide model (Padman and others, 2002; Howard and others, 2019) used to generate the prediction in  
536 Figs. 11 and 12, is available at <https://www.usap-dc.org/view/dataset/601235>.

537 A list of hardware components and data logger code will be made available on GitHub prior to publication.

## 539 9 ACKNOWLEDGEMENTS

540 HS is supported by the Antarctica New Zealand Doctoral Scholarship and the University of Otago Doctoral Schol-  
541 arship. The field campaign was supported by the Marsden Fund (grant number UOO052) awarded to DJP. We  
542 express our gratitude to Antarctica New Zealand and the staff at Scott Base for logistical support. We also express  
543 our appreciation to the staff at Mario Zucchelli Station for supporting both logistical and field operations, and for  
544 assistance to install a temporary base station. We thank Brent Pooley for fabricating the ground plates used for  
545 the patch antennas, and the School of Surveying, University of Otago, for lending the Trimble GNSS equipment.  
546 The authors gratefully acknowledge T. Takasu for their contribution to developing the open-source GNSS processing  
547 software RTKLIB.

## 548 REFERENCES

- 549 Alkan RM, Erol S and Mutlu B (2022) Real-time multi-GNSS Precise Point Positioning using IGS-RTS products in Antarctic  
550 region. *Polar Science*, **32** (doi: 10.1016/J.POLAR.2022.100844)
- 551 AllTerra (2023) GPS/GNSS Systems - Surveying Equipment - Products (Accessed:  
552 <https://allterracentral.com/products.html/survey-equipment/gps-systems.html>)
- 553 Arzeno IB, Beardsley RC, Limeburner R, Owens B, Padman L, Springer SR, Stewart CL and Williams MJ (2014) Ocean  
554 variability contributing to basal melt rate near the ice front of Ross Ice Shelf, Antarctica. *Journal of Geophysical Research: Oceans*, **119**, 4214–4233 (doi: 10.1002/2014JC009792)
- 556 Banville S, Hassen E, Lamothe P, Farinaccio J, Donahue B, Mireault Y, Goudarzi MA, Collins P, Ghoddousi-Fard R and  
557 Kamali O (2021) Enabling ambiguity resolution in CSRS-PPP. *Navigation*, **68**, 433–451 (doi: 10.1002/NAVI.423)

- 558 Benton CJ and Mitchell CN (2011) Isolating the multipath component in GNSS signal-to-noise data and locating reflecting  
559 objects. *Radio Science*, **46** (doi: 10.1029/2011RS004767)
- 560 Brenner AC, DiMarzio JP and Zwally HJ (2007) Precision and accuracy of satellite radar and laser altimeter data over the con-  
561 tinental ice sheets. *IEEE Transactions on Geoscience and Remote Sensing*, **45**, 321–331 (doi: 10.1109/TGRS.2006.887172)
- 562 Brunt KM, King MA, Fricker HA and MacAyeal DR (2010) Flow of the Ross Ice Shelf, Antarctica, is modulated by the ocean  
563 tide. *Journal of Glaciology*, **56**, 157–161 (doi: 10.3189/002214310791190875)
- 564 Brunt KM, Neumann TA and Larsen CF (2019) Assessment of altimetry using ground-based GPS data from the 88S Traverse,  
565 Antarctica, in support of ICESat-2. *Cryosphere*, **13**, 579–590 (doi: 10.5194/TC-13-579-2019)
- 566 Chagas AM (2018) Haves and have nots must find a better way: The case for open scientific hardware. *PLOS Biology*, **16**,  
567 e3000014 (doi: 10.1371/JOURNAL.PBIO.3000014)
- 568 Cooley J, Winberry P, Koutnik M and Conway H (2019) Tidal and spatial variability of flow speed and seismicity near the  
569 grounding zone of Beardmore Glacier, Antarctica. *Annals of Glaciology*, **60**, 37–44 (doi: 10.1017/aog.2019.14)
- 570 Dabovic P, Linty N and Dovis F (2020) Analysis of multi-constellation GNSS PPP solutions under phase scintillations at high  
571 latitudes. *Applied Geomatics*, **12**, 45–52 (doi: 10.1007/S12518-019-00269-4/TABLES/7)
- 572 Deng Z, Fritzsche M, Nischan T and Bradke M (2016) Multi-GNSS Ultra Rapid Orbit-, Clock- EOP Product Series, GFZ  
573 Data Services (doi: 10.5880/GFZ.1.1.2016.003)
- 574 Di M, Guo B, Ren J, Wu X, Zhang Z, Liu Y, Liu Q and Zhang A (2022) GNSS Real-Time Precise Point Positioning in Arctic  
575 Northeast Passage. *Journal of Marine Science and Engineering*, **10**, 1345 (doi: 10.3390/JMSE10101345)
- 576 Geng J, Teferle FN, Meng X and Dodson AH (2010) Kinematic precise point positioning at remote marine platforms. *GPS  
577 Solutions*, **14**, 343–350 (doi: 10.1007/s10291-009-0157-9)
- 578 GNSS OEM (2023) GNSS RTK Multiband Antennas: L1/L2/L5 GPS, G1/G2/G3 GLONASS, B1/B2/B3 BDS, Galileo  
579 E1/E5/E6 38dB Survey Antenna for RTK Base station. Available at: <https://gnss.store/gnss-rtk-multiband-antennas/140-elt0123.html> (Last accessed: August 20, 2023)
- 581 Greene CA, Gardner AS and Andrews LC (2020) Detecting seasonal ice dynamics in satellite images. *The Cryosphere*, **14**,  
582 4365–4378 (doi: 10.5194/tc-14-4365-2020)
- 583 Hamza V, Stopar B, Ambrožič T, Turk G and Sterle O (2020) Testing Multi-Frequency Low-Cost GNSS Receivers for Geodetic  
584 Monitoring Purposes. *Sensors 2020, Vol. 20, Page 4375*, **20**, 4375 (doi: 10.3390/S20164375)

- 585 Hohensinn R, Stauffer R, Glaner MF, Pinzón IDH, Vuadens E, Rossi Y, Clinton J and Rothacher M (2022) Low-Cost GNSS and  
586 Real-Time PPP: Assessing the Precision of the u-blox ZED-F9P for Kinematic Monitoring Applications. *Remote Sensing*,  
587 **14**, 5100 (doi: 10.3390/RS14205100/S1)
- 588 Horgan HJ, Hulbe C, Alley RB, Anandakrishnan S, Goodsell B, Taylor-Offord S and Vaughan MJ (2017) Poststagnation  
589 Retreat of Kamb Ice Stream's Grounding Zone. *Geophysical Research Letters*, **44**, 9815–9822 (doi: 10.1002/2017GL074986)
- 590 Howard SL, Padman L and Erofeeva S (2019) CATS2008: Circum-Antarctic Tidal Simulation version 2008 (Accessed:  
591 <https://doi.org/10.15784/601235>)
- 592 Huang MH, Lopez KU and Olsen KG (2022) Icequake-Magnitude Scaling Relationship Along a Rift Within the Ross Ice Shelf,  
593 Antarctica. *Geophysical Research Letters*, **49**, e2022GL097961 (doi: 10.1029/2022GL097961)
- 594 Hugentobler U and Montenbruck O (2017) Satellite Orbits and Attitude. In Teunissen PJG and Montenbruck O (eds.),  
595 *Springer Handbook of Global Navigation Satellite Systems*, 1st edition. 59–90 (doi: 10.1007/978-3-319-42928-1)
- 596 Hulbe CL and Whillans IM (1994) Evaluation of strain rates on Ice Stream B, Antarctica, obtained using GPS phase mea-  
597 surements. *Annals of Glaciology*, **20**, 254–262 (doi: 10.3189/172756494794587023)
- 598 Hulbe CL and Whillans IM (1997) Weak bands within Ice Stream B, West Antarctica. *Journal of Glaciology*, **43**, 377–386  
599 (doi: 10.3189/S002214300003495X)
- 600 Johnston G, Riddell A and Hausler G (2017) The International GNSS Service. In Teunissen PJG and Montenbruck O (eds.),  
601 *Springer Handbook of Global Navigation Satellite Systems*, 1st edition. 967–982 (doi: 10.1007/978-3-319-42928-1)
- 602 Jones DH, Robinson C and Gudmundsson GH (2016) A new high-precision and low-power GNSS receiver for long-term  
603 installations in remote areas. *Geosci. Instrum. Method. Data Syst.*, **5**, 65–73 (doi: 10.5194/gi-5-65-2016)
- 604 King MA, Watson CS and White D (2022) GPS Rates of Vertical Bedrock Motion Suggest Late Holocene Ice-Sheet Readvance  
605 in a Critical Sector of East Antarctica. *Geophysical Research Letters*, **49**, e2021GL097232 (doi: 10.1029/2021GL097232)
- 606 Klein E, Mosbeux C, Bromirski PD, Padman L, Bock Y, Springer SR and Fricker HA (2020) Annual cycle in flow of Ross Ice  
607 Shelf, Antarctica: contribution of variable basal melting. *Journal of Glaciology*, **66**, 861–875 (doi: 10.1017/JOG.2020.61)
- 608 Kouba J and Héroux P (2001) Precise Point Positioning Using IGS Orbit and Clock Products. *GPS Solutions*, **5**, 12–28 (doi:  
609 10.1007/PL00012883)
- 610 Kouba J, Lahaye F and Tétreault P (2017) Precise Point Positioning. In Teunissen PJG and Montenbruck O (eds.), *Springer*  
611 *Handbook of Global Navigation Systems*, 1st edition. 723–751 (doi: 10.1007/978-3-319-42928-1)

- 612 Krietemeyer A, van der Marel H, van de Giesen N and ten Veldhuis MC (2020) High Quality Zenith Tropospheric Delay  
613 Estimation Using a Low-Cost Dual-Frequency Receiver and Relative Antenna Calibration. *Remote Sensing*, **12**, 1393 (doi:  
614 10.3390/RS12091393)
- 615 Li M, Neumayer KH, Flechtner F, Lu B, Förste C, He K and Xu T (2019) Performance Assessment of Multi-GNSS Precise Veloc-  
616 ity and Acceleration Determination over Antarctica. *The Journal of Navigation*, **72**, 1–18 (doi: 10.1017/S0373463318000656)
- 617 Linty N, Dovis F and Alfonsi L (2018) Software-defined radio technology for GNSS scintillation analysis: bring Antarctica to  
618 the lab. **22**, 96 (doi: 10.1007/s10291-018-0761-7)
- 619 LINZ (2023) PositioNZ | Toitū Te Whenua - Land Information New Zealand (Accessed: [https://www.linz.govt.nz/products-](https://www.linz.govt.nz/products-services/geodetic/positionz)  
620 [services/geodetic/positionz](https://www.linz.govt.nz/products-services/geodetic/positionz))
- 621 Lutz F, Prior DJ, Still H, Bowman MH, Boucinkas B, Craw L, Fan S, Kim D, Mulvaney R, Thomas RE and Hulbe CL  
622 (2022) Ultrasonic and seismic constraints on crystallographic preferred orientations of the Priestley Glacier shear margin,  
623 Antarctica. *The Cryosphere*, **16**, 3313–3329 (doi: 10.5194/tc-16-3313-2022)
- 624 Manzini N, Orcesi A, Thom C, Brossault MA, Botton S, Ortiz M and Dumoulin J (2022) Performance analysis of low-cost  
625 GNSS stations for structural health monitoring of civil engineering structures. *Structure and Infrastructure Engineering*,  
626 **18**, 595–611 (doi: 10.1080/15732479.2020.1849320)
- 627 Matzka J, Stolle C, Yamazaki Y, Bronkalla O and Morschhauser A (2021) The Geomagnetic Kp Index and Derived Indices  
628 of Geomagnetic Activity. *Space Weather*, **19**, e2020SW002641 (doi: 10.1029/2020SW002641)
- 629 Minowa M, Podolskiy EA and Sugiyama S (2019) Tide-modulated ice motion and seismicity of a floating glacier tongue in  
630 East Antarctica. *Annals of Glaciology*, **60**, 57–67 (doi: 10.1017/aog.2019.25)
- 631 Montenbruck O, Steigenberger P, Prange L, Deng Z, Zhao Q, Perosanz F, Romero I, Noll C, Stürze A, Weber G, Schmid  
632 R, MacLeod K and Schaer S (2017) The Multi-GNSS Experiment (MGEX) of the International GNSS Service (IGS) –  
633 Achievements, prospects and challenges. *Advances in Space Research*, **59**, 1671–1697 (doi: 10.1016/J.ASR.2017.01.011)
- 634 Nie W, Rovira-Garcia A, Li M, Fang Z, Wang Y, Zheng D and Xu T (2022) The Mechanism for GNSS-Based Kinematic  
635 Positioning Degradation at High-Latitudes Under the March 2015 Great Storm. *Space Weather*, **20**, e2022SW003132 (doi:  
636 10.1029/2022SW003132)
- 637 Nie Z, Liu F and Gao Y (2020) Real-time precise point positioning with a low-cost dual-frequency GNSS device. *GPS Solutions*,  
638 **24**, 9 (doi: 10.1007/s10291-019-0922-3)
- 639 Nievinski FG and Larson KM (2014) Inverse modeling of GPS multipath for snow depth estimation - Part I: Formulation and  
640 simulations. *IEEE Transactions on Geoscience and Remote Sensing*, **52**, 6555–6563 (doi: 10.1109/TGRS.2013.2297681)

- 641 NOAA (2023) Geomagnetic KP and AP Indices (Accessed: [https://www.ngdc.noaa.gov/stp/geomag/kp\\_ap.html](https://www.ngdc.noaa.gov/stp/geomag/kp_ap.html))
- 642 Noll CE (2010) The crustal dynamics data information system: A resource to support scientific analysis using space geodesy.  
643 *Advances in Space Research*, **45**, 1421–1440 (doi: 10.1016/J.ASR.2010.01.018)
- 644 Notti D, Cina A, Manzino A, Colombo A, Bendea IH, Mollo P and Giordan D (2020) Low-Cost GNSS Solution for Con-  
tinuous Monitoring of Slope Instabilities Applied to Madonna Del Sasso Sanctuary (NW Italy). *Sensors*, **20**, 289 (doi:  
646 10.3390/S20010289)
- 647 Odijk D and Wanninger L (2017) Differential Positioning. In Teunissen PJG and Montenbruck O (eds.), *Springer Handbook  
648 of Global Navigation Satellite Systems*, 1st edition. 753–780 (doi: 10.1007/978-3-319-42928-1)
- 649 Odolinski R (2012) Temporal correlation for network RTK positioning. *GPS Solutions*, **16**, 147–155 (doi: 10.1007/S10291-011-  
650 0213-0/TABLES/7)
- 651 Odolinski R and Teunissen PJ (2016) Single-frequency, dual-GNSS versus dual-frequency, single-GNSS: a low-cost and high-  
652 grade receivers GPS-BDS RTK analysis. *Journal of Geodesy*, **90**, 1255–1278 (doi: 10.1007/S00190-016-0921-X)
- 653 Odolinski R and Teunissen PJ (2017) Low-cost, 4-system, precise GNSS positioning: a GPS, Galileo, BDS and QZSS  
654 ionosphere-weighted RTK analysis. *Measurement Science and Technology*, **28**, 125801 (doi: 10.1088/1361-6501/AA92EB)
- 655 Odolinski R and Teunissen PJ (2020) Best integer equivariant estimation: performance analysis using real data collected by  
656 low-cost, single- and dual-frequency, multi-GNSS receivers for short- to long-baseline RTK positioning. *Journal of Geodesy*,  
657 **94**, 1–17 (doi: 10.1007/S00190-020-01423-2/TABLES/4)
- 658 Odolinski R, Odijk D and Teunissen PJ (2014) Combined GPS and BeiDou Instantaneous RTK Positioning. *Navigation*, **61**,  
659 135–148 (doi: 10.1002/NAVI.61)
- 660 Odolinski R, Teunissen PJ and Odijk D (2015a) Combined BDS, Galileo, QZSS and GPS single-frequency RTK. *GPS Solutions*,  
661 **19**, 151–163 (doi: 10.1007/S10291-014-0376-6/FIGURES/10)
- 662 Odolinski R, Teunissen PJ and Odijk D (2015b) Combined GPS + BDS for short to long baseline RTK positioning. *Measure-  
663 ment Science and Technology*, **26** (doi: 10.1088/0957-0233/26/4/045801)
- 664 Oellermann M, Jolles JW, Ortiz D, Seabra R, || TW, Wilson H and Tanner RL (2022) Open Hardware in Science: The Benefits  
665 of Open Electronics. *Integrative and Comparative Biology*, **62**, 1061–1075 (doi: 10.1093/ICB/ICAC043)
- 666 Padman L, Fricker HA, Coleman R, Howard S and Erofeeva L (2002) A new tide model for the Antarctic ice shelves and seas.  
667 *Annals of Glaciology*, **34**, 247–254 (doi: 10.3189/172756402781817752)

- 668 Paziewski J (2022) Multi-constellation single-frequency ionospheric-free precise point positioning with low-cost receivers. *GPS  
669 Solutions*, **26**, 1–11 (doi: 10.1007/S10291-021-01209-9/FIGURES/10)
- 670 Paziewski J and Wielgosz P (2017) Investigation of some selected strategies for multi-GNSS instantaneous RTK positioning.  
671 *Advances in Space Research*, **59**, 12–23 (doi: 10.1016/j.asr.2016.08.034)
- 672 Paziewski J, Høeg P, Sieradzki R, Jin Y, Jarmolowski W, Hoque MM, Berdermann J, Hernandez-Pajares M, Wielgosz P,  
673 Lyu H, Miloch WJ and Orús-Pérez R (2022) The implications of ionospheric disturbances for precise GNSS positioning in  
674 Greenland. *Journal of Space Weather and Space Climate*, **12**, 33 (doi: 10.1051/SWSC/2022029)
- 675 Pratap B, Dey R, Matsuoka K, Moholdt G, Lindbäck K, Goel V, Laluraj CM and Thamban M (2022) Three-decade spatial  
676 patterns in surface mass balance of the Nivlisen Ice Shelf, central Dronning Maud Land, East Antarctica. *Journal of  
677 Glaciology*, **68**, 174–186 (doi: 10.1017/JOG.2021.93)
- 678 Punzet S and Eibert TF (2023) Impact of Additional Antenna Groundplanes on RTK-GNSS Positioning Accuracy of UAVs.  
679 *Advances in Radio Science*, **20**, 23–28 (doi: 10.5194/ARS-20-23-2023)
- 680 Richter A, Popov SV, Fritzsche M, Lukin VV, Matveev AY, Ekaykin AA, Lipenkov VY, Fedorov DV, Eberlein L, Schröder L,  
681 Ewert H, Horwath M and Dietrich R (2014) Height changes over subglacial Lake Vostok, East Antarctica: Insights from  
682 GNSS observations. *Journal of Geophysical Research: Earth Surface*, **119**, 2460–2480 (doi: 10.1002/2014JF003228)
- 683 Rignot E, Mouginot J and Scheuchl B (2016) *MEaSURES Antarctic Grounding Line from Differential Satellite Radar  
684 Interferometry, Version 2*. NASA National Snow and Ice Data Center Distributed Active Archive Center (doi:  
685 10.5067/IKBWW4RYHF1Q)
- 686 Romero-Andrade R, Trejo-Soto ME, Vega-Ayala A, Hernández-Andrade D, Vázquez-Ontiveros JR and Sharma G (2021)  
687 Positioning Evaluation of Single and Dual-Frequency Low-Cost GNSS Receivers Signals Using PPP and Static Relative  
688 Methods in Urban Areas. *Applied Sciences*, **11**, 10642 (doi: 10.3390/APP112210642)
- 689 Schröder L, Richter A, Fedorov DV, Eberlein L, Brovkov EV, Popov SV, Knöfel C, Horwath M, Dietrich R, Matveev AY,  
690 Scheinert M and Lukin VV (2017) Validation of satellite altimetry by kinematic GNSS in central East Antarctica. *Cryosphere*,  
691 **11**, 1111–1130 (doi: 10.5194/TC-11-1111-2017)
- 692 Schüler T (2006) Impact of systematic errors on precise long-baseline kinematic GPS positioning. *GPS Solutions*, **10**, 108–125  
693 (doi: 10.1007/S10291-005-0012-6)
- 694 Šegina E, Peternel T, Urbančič T, Realini E, Zupan M, Jež J, Caldera S, Gatti A, Tagliaferro G, Consoli A, González JR and  
695 Auflíč MJ (2020) Monitoring Surface Displacement of a Deep-Seated Landslide by a Low-Cost and near Real-Time GNSS  
696 System. *Remote Sensing*, **12**, 3375 (doi: 10.3390/RS12203375)

- 697 Siegfried MR, Fricker HA, Carter SP and Tulaczyk S (2016) Episodic ice velocity fluctuations triggered by a subglacial flood  
698 in West Antarctica. *Geophysical Research Letters*, **43**, 2640–2648 (doi: 10.1002/2016GL067758)
- 699 Spikes VB, Csathó BM and Whillans IM (2003) Laser profiling over Antarctic ice streams: Methods and accuracy. *Journal of*  
700 *Glaciology*, **49**, 315–322 (doi: 10.3189/172756503781830737)
- 701 Steigenberger P and Montenbruck O (2020) In Villiger A and Dach R (eds.), *Multi-GNSS Working Group Technical Report*  
702 2019. 219–229 (doi: 10.7892/BORIS.144003)
- 703 Still H, Hulbe C, Forbes M, Prior DJ, Bowman MH, Boucinha B, Craw L, Kim D, Lutz F, Mulvaney R and Thomas RE  
704 (2022) Tidal modulation of a lateral shear margin: Priestley Glacier, Antarctica. *Frontiers in Earth Science*, **10**, 687 (doi:  
705 10.3389/feart.2022.828313)
- 706 Takasu T (2013) RTKLIB Ver. 2.4.2 Manual: RTKLIB: An Open Source Program Package for GNSS Positioning (Accessed:  
707 [https://www.rtklib.com/prog/manual\\_2.4.2.pdf](https://www.rtklib.com/prog/manual_2.4.2.pdf))
- 708 Takasu T and Yasuda A (2009) Development of the low-cost RTK-GPS receiver with an open source program package RTKLIB.  
709 *International symposium on GPS/GNSS.*, **1**, 1–6 (doi: [https://gpspp.sakura.ne.jp/paper2005/isgps\\_2009\\_rklib.pdf](https://gpspp.sakura.ne.jp/paper2005/isgps_2009_rklib.pdf))
- 710 Teunissen PJG, Odolinski R and Odijk D (2014) Instantaneous BeiDou+GPS RTK positioning with high cut-off elevation  
711 angles. *Journal of Geodesy*, **88**, 335–350 (doi: 10.1007/s00190-013-0686-4)
- 712 Thomas ID, King MA, Bentley MJ, Whitehouse PL, Penna NT, Williams SD, Riva RE, Lavallee DA, Clarke PJ, King EC,  
713 Hindmarsh RC and Koivula H (2011) Widespread low rates of Antarctic glacial isostatic adjustment revealed by GPS  
714 observations. *Geophysical Research Letters*, **38** (doi: 10.1029/2011GL049277)
- 715 Thomas RE, Negrini M, Prior DJ, Mulvaney R, Still H, Bowman MH, Craw L, Fan S, Hubbard B, Hulbe C, Kim D and Lutz  
716 F (2021) Microstructure and Crystallographic Preferred Orientations of an Azimuthally Oriented Ice Core from a Lateral  
717 Shear Margin: Priestley Glacier, Antarctica. *Frontiers in Earth Science*, **9**, 1084 (doi: 10.3389/feart.2021.702213)
- 718 Tidey E and Odolinski R (2023) Low-cost multi-GNSS, single-frequency RTK averaging for marine applications: accurate  
719 stationary positioning and vertical tide measurements. *Marine Geodesy*, 1–26 (doi: 10.1080/01490419.2023.2208289)
- 720 Tunini L, Zuliani D and Magrin A (2022) Applicability of Cost-Effective GNSS Sensors for Crustal Deformation Studies.  
721 *Sensors*, **22**, 350 (doi: 10.3390/S22010350)
- 722 U-blox (2019) GNSS antennas: RF design considerations for u-blox GNSS receivers. Available at: [https://content.u-blox.com/sites/default/files/products/documents/GNSS-Antennas\\_AppNote\\_%28UBX-15030289%29.pdf](https://content.u-blox.com/sites/default/files/products/documents/GNSS-Antennas_AppNote_%28UBX-15030289%29.pdf) (Last accessed:  
723 1 June, 2023)

Still and others: Low-cost GNSS positioning in Antarctica

42

- 725 U-blox (2022a) ANN-MB series Multi-band, high precision GNSS antennas. Available at: [https://content.u-blox.com/sites/default/files/documents/ANN-MB\\_DataSheet\\_UBX-18049862.pdf](https://content.u-blox.com/sites/default/files/documents/ANN-MB_DataSheet_UBX-18049862.pdf) (Last accessed: 1 June, 2023)
- 727 U-blox (2022b) U-center GNSS evaluation software for Windows. Available at: [https://content.u-blox.com/sites/default/files/u-center\\_Userguide\\_UBX-13005250.pdf](https://content.u-blox.com/sites/default/files/u-center_Userguide_UBX-13005250.pdf) (Last accessed: 1 June, 2023)
- 729 U-blox (2022c) ZED-F9P-04B u-blox F9 high precision GNSS module. Available at: [https://content.u-blox.com/sites/default/files/ZED-F9P-04B\\_DataSheet\\_UBX-21044850.pdf](https://content.u-blox.com/sites/default/files/ZED-F9P-04B_DataSheet_UBX-21044850.pdf) (Last accessed: 1 June, 2023)
- 731 U-blox (2023) ZED-F9P module | u-blox. Available at: <https://www.u-blox.com/en/product/zed-f9p-module> (Last accessed: 1 June, 2023)
- 733 Willis MJ (2008) Technologies to Operate Year-Round Remote Global Navigation Satellite System (GNSS) Stations in Extreme Environments. In Capra A and Dietrich R (eds.), *Geodetic and Geophysical Observations in Antarctica*, 1st edition. 11–35  
734 (doi: 10.1007/978-3-540-74882-3\_2)
- 736 Wolf P and Ghilani C (2006) *Elementary Surveying: An Introduction to Geomatics*. Pearson, 11th edition
- 737 Xue C, Psimoulis P, Zhang Q and Meng X (2021) Analysis of the performance of closely spaced low-cost multi-GNSS receivers.  
738 *Applied Geomatics*, **13**, 415–435 (doi: 10.1007/S12518-021-00361-8/FIGURES/21)
- 739 Xue C, Psimoulis PA and Meng X (2022) Feasibility analysis of the performance of low-cost GNSS receivers in monitoring  
740 dynamic motion. *Measurement*, **202**, 111819 (doi: 10.1016/J.MEASUREMENT.2022.111819)
- 741 Yong C, Odolinski R, Zaminpardaz S, Moore M, Rubinov E, Er J and Denham M (2021) Instantaneous, Dual-Frequency,  
742 Multi-GNSS Precise RTK Positioning Using Google Pixel 4 and Samsung Galaxy S20 Smartphones for Zero and Short  
743 Baselines. *Sensors*, **21**, 8318 (doi: 10.3390/S21248318)
- 744 Zanutta A, Negusini M, Vittuari L, Cianfarra P, Salvini F, Mancini F, Sterzai P, Dubbini M, Galeandro A and Capra A (2017)  
745 Monitoring geodynamic activity in the Victoria Land, East Antarctica: Evidence from GNSS measurements. *Journal of  
746 Geodynamics*, **110**, 31–42 (doi: 10.1016/J.JOG.2017.07.008)
- 747 Zhang Q, Chen Z, Cui Y, Zheng X, Rong F, Sun Y and Gao L (2020) A refined metric for multi-GNSS constellation availability  
748 assessment in polar regions. *Advances in Space Research*, **66**, 655–670 (doi: 10.1016/J.ASR.2020.04.033)
- 749 Zumberge JF, Heflin MB, Jefferson DC, Watkins MM and Webb FH (1997) Precise point positioning for the efficient and  
750 robust analysis of GPS data from large networks. *Journal of Geophysical Research: Solid Earth*, **102**, 5005–5017 (doi:  
751 10.1029/96JB03860)